

Testing Fundamental Physics with Astrophysical Transients

Jun-Jie Wei^{1,2,*}, Xue-Feng Wu^{1,2,†}

1. Purple Mountain Observatory, Chinese Academy of Sciences, Nanjing 210023, China

2. School of Astronomy and Space Sciences, University of Science and Technology of China, Hefei 230026, China

Corresponding authors. E-mail: *jjwei@pmo.ac.cn, †xfwu@pmo.ac.cn

Explosive astrophysical transients at cosmological distances can be used to place precision tests of the basic assumptions of relativity theory, such as Lorentz invariance, the photon zero-mass hypothesis, and the weak equivalence principle (WEP). Signatures of Lorentz invariance violations (LIV) include vacuum dispersion and vacuum birefringence. Sensitive searches for LIV using astrophysical sources such as gamma-ray bursts, active galactic nuclei, and pulsars are discussed. The most direct consequence of a nonzero photon rest mass is a frequency dependence in the velocity of light propagating in vacuum. A detailed representation of how to obtain a combined severe limit on the photon mass using fast radio bursts at different redshifts through the dispersion method is presented. The accuracy of the WEP has been well tested based on the Shapiro time delay of astrophysical messengers traveling through a gravitational field. Some caveats of Shapiro delay tests are discussed. In this article, we review and update the status of astrophysical tests of fundamental physics.

Keywords Astroparticle physics, Gravitation, Astrophysical transients

PACS numbers 04.60.Pp, 95.30.Sf, 98.70.Dk, 98.70.Rz

Contents

1	Introduction	1
2	Astrophysical tests of LIV	3
2.1	Vacuum dispersion from LIV	3
2.1.1	General formulae	3
2.1.2	Present results	3
2.2	Vacuum birefringence from LIV	8
2.2.1	General formulae	8
2.2.2	Present constraints	9
2.2.3	Comparison with time-of-flight limits	10
3	Astrophysical bounds on the photon mass	10
3.1	Dispersion from a nonzero photon mass	10
3.2	Dispersion from the plasma effect	12
3.3	Combined limits on the photon mass	13
4	Astrophysical tests of the WEP	15
4.1	Arrival time tests of the WEP	16
4.2	Polarization tests of the WEP	17
5	Summary and future prospect	18
	References	19

1 Introduction

Einstein's theory of special and general relativity is a major pillar of modern physics, with a wide application in astrophysics. It is, therefore, of great scientific sig-

nificance to test the validity of the basic assumptions of relativity theory, such as Lorentz invariance, the photon zero-mass hypothesis, and the weak equivalence principle (WEP). When the terrestrial conditions eventually impose some limitations, the extreme features of astrophysical phenomena afford the ideal testbeds for obtaining higher precision tests of the fundamental laws of physics. Lorentz invariance, which is the fundamental symmetry of Einstein's special relativity, says that the relevant physical laws of a non-accelerating physical system are invariant under Lorentz transformation. However, deviations from Lorentz invariance at a natural energy scale are suggested in many quantum gravity (QG) theories seeking to unify general relativity and quantum mechanics, such as loop quantum gravity [1, 2], double special relativity [3–6], and superstring theory [7]. This natural scale, referred to as the “QG energy scale” E_{QG} , is generally supposed to be around the Planck energy $E_{\text{Pl}} = \sqrt{\hbar c^5/G} \simeq 1.22 \times 10^{19}$ GeV [7–13]. The dedicated experimental tests of Lorentz invariance may therefore help to clear the path to a grand unified theory. A compilation of various recent experimental tests may be found in Ref. [14]. Although any violations of Lorentz symmetry are predicted to be tiny at observable energies $\ll E_{\text{Pl}}$, they can accumulate to measurable levels over large distances. Therefore, astrophysical measurements involving long baselines can provide sensitive probes of Lorentz invariance violation (LIV). In the photon sector, the potential signatures of LIV include vacuum dispersion and

vacuum birefringence [15]. Vacuum dispersion would produce an energy-dependent speed of light that in turn would translate into differences in the arrival time of photons with different energies traveling over cosmological distances. Lorentz invariance can therefore be tested using astrophysical time-of-flight measurements (e.g., Refs. [15–35]). Similarly, the effect of vacuum birefringence would accumulate over astrophysical distances resulting in a detectable rotation of the polarization vector of linearly polarized emission as a function of energy. Thus, Lorentz invariance can also be probed with astrophysical polarization measurements (e.g., Refs. [36–55]). Typically, polarization measurements place more stringent constraints on LIV. This can be understood by the fact that polarization measurements are more sensitive than time-of-flight measurements by a factor $\propto 1/E$, where E is the energy of the photon [20]. However, numerous predicted Lorentz-violating signals have no vacuum birefringence, so constraints from time-of-flight measurements are indispensable in an extensive search for non-birefringent effects.

The postulate that all electromagnetic waves travel in vacuum at the constant speed c is one of the foundations of Maxwell's electromagnetism and Einstein's special relativity. The constancy of light speed implies that the quantum of light, or photon, should be massless. The validity of this postulate can therefore be tested by searching for a rest mass of the photon. However, none of the experiments so far could confirm that the photon rest mass is absolutely zero. Based on the uncertainty principle, when using the age of the universe ($T \sim 10^{10}$ yr), there is an ultimate upper limit on the photon rest mass, i.e., $m_\gamma \leq \hbar/Tc^2 \approx 10^{-69}$ kg [56, 57]. The best one can hope to do is to set ever tighter limits on m_γ and push the experimental results even closer to the ultimate upper limit. In theory, a nonzero photon rest mass can be accommodated into electromagnetism through the Proca equations. Using them, some possible visible effects associated with a massive photon have been carefully studied, which open the door to useful approaches for terrestrial experiments or astrophysical observations aimed at placing upper limits on the photon rest mass (see Refs. [56–60] for reviews). To date, the experimental methods for constraining m_γ include the frequency dependence of the speed of light ($m_\gamma \leq 5.1 \times 10^{-51}$ kg) [61–72], Coulomb's inverse square law ($m_\gamma \leq 1.6 \times 10^{-50}$ kg) [73], Ampère's law ($m_\gamma \leq (8.4 \pm 0.8) \times 10^{-49}$ kg) [74], torsion balance ($m_\gamma \leq 1.2 \times 10^{-54}$ kg) [75–78], gravitational deflection of electromagnetic waves ($m_\gamma \leq 10^{-43}$ kg) [79, 80], Jupiter's magnetic field ($m_\gamma \leq 8 \times 10^{-52}$ kg) [81], magnetohydrodynamic phenomena of the solar wind ($m_\gamma \leq 1.4 \times 10^{-49} - 3.4 \times 10^{-51}$ kg) [82–84], cosmic magnetic fields ($m_\gamma \leq 10^{-62}$ kg) [85–87], supermassive black-hole spin ($m_\gamma \leq 10^{-56} - 10^{-58}$ kg) [88], spindown of a

white-dwarf pulsar ($m_\gamma \leq (6.3 - 9.6) \times 10^{-53}$ kg) [89], and so on. Among these methods, the most direct and robust one is to detect a possible frequency dependence in the velocity of light. In this article, we will review the photon mass limits from the dispersion of electromagnetic waves of astrophysical sources.

Einstein's WEP states that any freely falling, uncharged test body will follow a trajectory, independent of its internal structure and composition [90, 91]. It is the basic ingredient of general relativity and other metric theories of gravity. The most famous tests of the WEP are the Eötvös-type experiments, which compare the accelerations of two laboratory-sized objects consisted of different composition in a known gravitational field (see Ref. [91] for a review). For laboratory-sized objects with macroscale masses, the accuracy of the WEP can be tested in a Newtonian context. However, the motion of test particles (like photons or neutrinos) in a gravitational field is not precisely described by Newtonian dynamics. As such, the parameterized post-Newtonian (PPN) formalism has been developed to describe exactly their motion. Each theory of gravitation satisfying the WEP is specified by a set of PPN parameters. The WEP can then also be tested by massless (or negligible rest-mass) particles in the context of the PPN formalism and any possible deviation from WEP is characterized by the PPN parameter, γ , of a particular gravity theory. Here γ reflects the level of space curved by unit rest mass [90, 91]. In general relativity, γ is predicted to be strictly 1. The determination of the absolute γ value has reached high precision. The light deflection measurements through very-long-baseline radio interferometry yielded an agreement with general relativity to 0.01 percent, i.e., $\gamma - 1 = (-0.8 \pm 1.2) \times 10^{-4}$ [92, 93]. The radar time-delay measurement from the Cassini spacecraft obtained a more stringent constraint $\gamma - 1 = (2.1 \pm 2.3) \times 10^{-5}$ [94]. Regardless of the absolute value of γ , all metric theories of gravity incorporating the WEP predict that different species of messenger particles (photons, neutrinos, and gravitational waves (GWs)), or the same species of particles but with different internal properties (e.g., energies or polarization states), traveling through the same gravitational fields, must follow identical trajectories and undergo the same γ -dependent Shapiro delay [95]. To test the WEP, therefore, the issue is not whether the value of γ is very nearly unity, but whether it is the same for all test particles. The Shapiro time delay of test particles emitted from the same astrophysical sources has been widely applied to constrain a possible violation of the WEP through the relative differential variations of the γ values (e.g., [96–102]).

In this review, we summarize the current status on astrophysical tests of fundamental physics and attempt to chart the future of the subject. In Section 2, we review

two common astrophysical approaches to testing the LIV effects. Section 3 is dedicated to discuss astrophysical bounds on the photon rest mass through the measurement of the frequency dependence of the speed of light. In Section 4, we focus on tests of the WEP through the Shapiro (gravitational) time delay effect. Finally, a summary and future prospect are presented in Section 5.

2 Astrophysical tests of LIV

Various QG theories that extend beyond the standard model predict violations of Lorentz invariance at energies approaching the Planck scale [7–13]. The existence of LIV can produces an energy-dependent vacuum dispersion of light, which leads to time delays between promptly emitted photons with different energies, as well as an energy-dependent rotation of the polarization plane of linearly polarized photons resulting from vacuum birefringence. In this section, we first review the recent achievements in sensitivity of vacuum dispersion time-of-flight measurements. Then the progress on LIV limits from astrophysical polarization measurements is discussed.

2.1 Vacuum dispersion from LIV

2.1.1 General formulae

Several QG theories proposed to describe quantum spacetime, predict the granularity of space and time. For example, string theory that remove the point-like nature of the particles by introducing to each of them a (mono)-dimensional extension: the string (see, e.g., Smolin [103] for reviews). Loop quantum gravity that question the continuousness and smoothness of space-time quantizing it into discrete energy levels like those observed in the classical quantum-mechanical systems to construct a complex geometric structure called spin networks (see, e.g., Rovelli [104] for reviews). In both proposed theories emerge a minimal length for physical space (and time), although with different and somewhat opposite theoretical approaches [105]. The minimal spatial and temporal scales associated to the quantization are in terms of standard units: $l_P \sim \sqrt{\hbar G/c^3} \sim 10^{-33}$ cm and $t_P \sim \sqrt{\hbar G/c^5} \sim 10^{-43}$ s for the Planck length and time, respectively. A significant class of QG theories predict that the propagation of photons through this discrete spacetime might exhibit a non-trivial dispersion relation in vacuum [16], corresponding to the possible violation or break of the Lorentz invariance via an energy-dependent speed of light. In vacuum, the LIV-induced modifications to the dispersion relation of photons can

be described using a Taylor series expansion:

$$E^2 \simeq p^2 c^2 \left[1 - \sum_{n=1}^{\infty} s_{\pm} \left(\frac{E}{E_{\text{QG},n}} \right)^n \right], \quad (1)$$

where p is the photon momentum, E_{QG} is the hypothetical energy scale at which QG effects would become significant, and $s_{\pm} = \pm 1$ is a theory-dependent factor. For $E \ll E_{\text{QG}}$, the sum is dominated by the lowest-order term in the series. Considering only the lowest-order dominant term, the photon group velocity can therefore be expressed by

$$v(E) = \frac{\partial E}{\partial p} \approx c \left[1 - s_{\pm} \frac{n+1}{2} \left(\frac{E}{E_{\text{QG},n}} \right)^n \right], \quad (2)$$

where $n = 1$ and $n = 2$ correspond to the linear and quadratic LIV, respectively. The coefficient $s_{\pm} = +1$ ($s_{\pm} = -1$) stands for a decrease (increase) in the photon speed along with increasing photon energy (also refers to the “subluminal” and “superluminal” scenarios).

Because of the energy dependence of $v(E)$, two photons with different observer-frame energies ($E_h > E_l$) emitted simultaneously from the same astrophysical source at redshift z would arrive at the observer at different times. Taking account of the cosmological expansion, we derive the expression of the LIV-induced time delay [19]:

$$\begin{aligned} \Delta t_{\text{LIV}} &= t_h - t_l \\ &= s_{\pm} \frac{1+n}{2H_0} \frac{E_h^n - E_l^n}{E_{\text{QG},n}^n} \int_0^z \frac{(1+z')^n dz'}{\sqrt{\Omega_m(1+z')^3 + \Omega_\Lambda}}, \end{aligned} \quad (3)$$

where t_h and t_l , respectively, denote the arrival times of the high-energy and low-energy photons, H_0 is the Hubble constant, and Ω_m and Ω_Λ are the matter energy density and the vacuum energy density (parameters of the flat Λ CDM model). Since the adopted energy range generally spans several orders of magnitude, one can approximate $(E_h^n - E_l^n) \approx E_h^n$. Adopting $z = 20$ as a firm upper limit for the redshift of any source, we find the LIV-induced time delay is $|\Delta t_{\text{LIV}}| \leq 0.5(E_h \text{ GeV}/\zeta)$ s for the linear ($n = 1$) LIV case and $|\Delta t_{\text{LIV}}| \leq 5.2 \times 10^{-19}(E_h \text{ GeV}/\zeta)^2$ s for the quadratic ($n = 2$) LIV case, where $E_h \text{ GeV} = E_h/(1 \text{ GeV})$ and $\zeta = E_{\text{QG}}/E_{\text{Pl}}$. These indicate that first order ($n = 1$) effects would lead to potentially observable delays, while second order ($n = 2$) effects are so tiny that it would be impossible to observe them with this time-of-flight technique.

2.1.2 Present results

Eq. (3) shows that the LIV-induced time delay increases with the energy of the photons and the distance of

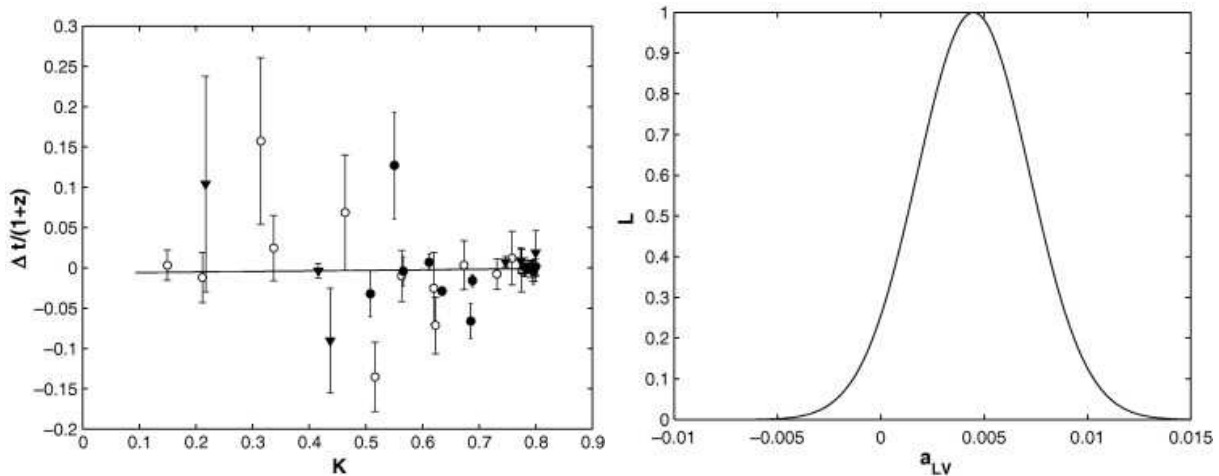


Fig. 1 Left panel: the rescaled time lags between two selected observer-frame energy bands from the full set of 35 GRBs with known redshifts observed until 2006 by BATSE (closed circles), HETE-2 (open circles) and Swift (triangles). Right panel: the likelihood function for the slope parameter a_{LV} . Reproduced from Ref. [106].

the source. A short timescale of the signal variability easily provides a reference time to measure the time delay. The higher the photon energy, the longer the source distance, and the shorter the time delay, the more stringent limits on the QG energy scale one can reach. Exploiting the rapid variations of gamma-ray emissions from astrophysical sources at large distances to constrain LIV was first proposed by Amelino-Camelia et al. [16]. At present, tests of LIV have been made using the observations of gamma-ray bursts (GRBs), active galactic nuclei (AGNs), and pulsars.

- Gamma-ray bursts

GRBs are among the most distant gamma-ray sources and their signals vary on subsecond timescales. As such, GRBs are identified as promising sources for LIV studies. There have been many searches for LIV through studies on the time-of-flight measurements of GRBs. Some of the pre-Fermi studies are those by Ellis et al. [107] using BATSE GRBs; by Boggs et al. [108] using RHESSI observations of GRB 021206; by Ellis et al. [18, 106] using BATSE, HETE-2, and Swift GRBs; by Rodríguez-Martínez et al. [109] using Konus-Wind and Swift observations of GRB 051221A; by Bolmont et al. [110] using HETE-2 GRBs; and by Lamon et al. [111] using INTEGRAL GRBs. Because of the unprecedented sensitivity for detecting the prompt high-energy GRB emission (up to tens of GeV) by the Fermi Large Area Telescope (LAT), more stringent constraints on LIV have been obtained using Fermi observations. These constraints include those by the Fermi Collaboration using GRBs 080916C [21] and 090510 [22]; by Xiao & Ma [112] using GRB 090510; and by Refs. [23–25, 28, 32, 113–117] using multiple Fermi GRBs. Particularly, Abdo et al. [22]

used the highest energy (31 GeV) photon of the short GRB 090510 detected by Fermi/LAT to constrain the linear LIV energy scale ($E_{QG,1}$). The burst has a redshift $z = 0.903$. This 31 GeV photon was detected 0.829 s after the Fermi Gamma-Ray Burst Monitor (GBM) trigger. If the 31 GeV photon was emitted at the beginning of the first GBM pulse, one has $\Delta t_{LIV} < 859$ ms, which gives the most conservative constraint $E_{QG,1} > 1.19E_{Pl}$. If the 31 GeV photon is associated with the contemporaneous < 1 MeV spike, one has $\Delta t_{LIV} < 10$ ms, which gives the least conservative constraint $E_{QG,1} > 102E_{Pl}$. We can see that the linear LIV models requiring $E_{QG,1} \leq E_{Pl}$ are disfavored by these results. Subsequently, Vasileiou et al. [25] used three statistical techniques to constrain the total degree of dispersion in the data of four LAT-detected GRBs. For the subluminal case, their most stringent limits are derived from GRB 090510 and are $E_{QG,1} > 7.6E_{Pl}$ and $E_{QG,2} > 1.3 \times 10^{11}$ GeV for linear and quadratic LIV, respectively. These limits improve previous constraints by a factor of ~ 2 . Recently, the Major Atmospheric Gamma Imaging Cherenkov (MAGIC) telescopes first detected GRB 190114C in the sub-TeV energy domain (i.e., 0.2–1 TeV), recording the highest energy photons ever observed from a GRB [118]. Using conservative assumptions on the possible intrinsic spectral and temporal emission properties, the MAGIC Collaboration searched for an energy dependence in the arrival time of the most energetic photons and presented competitive limits on the quadratic leading-order LIV-induced vacuum dispersion [33]. The resulting constraints from GRB 190114C are $E_{QG,2} > 6.3 \times 10^{10}$ GeV and $E_{QG,2} > 5.6 \times 10^{10}$ GeV for the subluminal and superluminal cases, respectively.

By using the arrival-time differences between high-energy and low-energy photons (the so-called spectral

lags) from GRBs, Lorentz invariance has been tested with unprecedented accuracy. Such time-of-flight tests, however, are subject to a bias related to a possible intrinsic time lag introduced from the unknown emission mechanism of the sources, which would enhance or cancel-out the delay caused by the LIV effects. That is, the method of the arrival-time difference is tempered by our ignorance concerning potential source-intrinsic effects. The first attempt to mitigate the intrinsic time lag problem was proposed by Ellis et al. [18, 106, 107], who suggested working on a large sample of GRBs with different redshifts. For each GRB, Ellis et al. [18] looked for the spectral lag in the light curves recorded in the chosen observer-frame energy bands 115–320 and 25–55 keV. To account for the poorly known intrinsic time lag, they fitted the observed spectral lags of 35 GRBs with the inclusion of a constant b_{sf} specified in the rest frame of the source. The observed arrival time delays thus have two contributions $\Delta t_{\text{obs}} = \Delta t_{\text{LIV}} + b_{\text{sf}}(1+z)$, reflecting the possible LIV effects and source-intrinsic effects [18]. Rescaling Δt_{obs} by a factor $(1+z)$, then one has a simple linear fitting function

$$\frac{\Delta t_{\text{obs}}}{1+z} = a_{\text{LV}} K + b_{\text{sf}}, \quad (4)$$

where

$$K = \frac{1}{(1+z)} \int_0^z \frac{(1+z')dz'}{h(z')} \quad (5)$$

is a function of redshift which depends on the cosmological model, the slope $a_{\text{LV}} = \Delta E / (H_0 E_{\text{QG}})$ is related to the QG energy scale, and the intercept b_{sf} denotes the possible unknown intrinsic time lag. In the standard flat Λ CDM model, the dimensionless expansion rate $h(z)$ is expressed as $h(z) = \sqrt{\Omega_m(1+z)^3 + \Omega_\Lambda}$. Note that the linear LIV ($n = 1$) in the subluminal case ($s_\pm = +1$) was considered in this work. Within a framework of the concordance Λ CDM model, a linear fit to the rescaled time lags extracted from 35 light curve pairs is shown in the left panel of Figure 1. The best-fit line corresponds to $\frac{\Delta t_{\text{obs}}}{1+z} = (0.0068 \pm 0.0067)K - (0.0065 \pm 0.0046)$ and the likelihood function for the slope parameter a_{LV} is presented in the right panel of Figure 1. The 95% confidence-level lower limit on the linear LIV energy scale derived from the likelihood function of a_{LV} is $E_{\text{QG}} \geq 1.4 \times 10^{16}$ GeV [106]. Going beyond the Λ CDM cosmology, Refs. [119, 120] extended this analysis to different cosmological models and showed that the result is insensitive to the adopted background cosmology. Subsequently, some cosmology-independent approaches were applied to probe the possible LIV effects [121, 122].

It should be noted that there are two limitations in the treatment of Ellis et al. [18]. First, they extracted spectral lags in the light curves between two fixed observer-frame energy bands. However, because different GRBs

have different redshift measurements, these two energy bands correspond to a different pair of energy bands in the source frame [123], thus potentially causing an artificial energy dependence to the extracted spectral lag and/or a systematic uncertainty to the search for LIV lags.¹ Ukwatta et al. [123] found that there is a large scatter in the correlation between observer-frame lags and source-frame lags for the same GRB sample, indicating that the observer-frame lag does not faithfully represent the source-frame lag. The first limitation of Ellis et al. treatment can be resolved by selecting two appropriate energy bands fixed in the rest frame and calculating the time lag for two projected observer-frame energy bands by the relation $E_{\text{observer}} = E_{\text{source}}/(1+z)$. Bernardini et al. [124] studied the source-frame spectral lags of 56 GRBs detected by Swift/Burst Alert Telescope (BAT). For each GRB, they extracted light curves for two observer-frame energy bands corresponding to the fixed energy bands in the source frame, i.e., 100–150 and 200–250 keV. These two particular source-frame energy bands were selected to ensure that the projected observer-frame energy bands (i.e., $[100 - 150]/(1+z)$ and $[200 - 250]/(1+z)$ keV) are within the detectable energy range of the BAT instrument (see Figure 2). For each extracted light-curve pairs, they used the discrete cross-correlation function to calculate the spectral lag. Note that the energy difference between the median-values of the two source-frame energy bands is fixed at 100 keV, whereas in the observer frame, the energy difference varies depending on the redshift of each burst. This is in contrast to the spectral lag extractions achieved in the observer frame, where the energy difference is treated as a constant [123]. Wei & Wu [31] first took advantage of the source-frame spectral lags of 56 Swift GRBs presented in Bernardini et al. [124] to investigate the LIV effects. For the subluminal case, the arrival-time difference of two photons with observer-frame energy difference ΔE that induced by the linear LIV reads:

$$\begin{aligned} \Delta t_{\text{LIV}} &= \frac{\Delta E}{H_0 E_{\text{QG}}} \int_0^z \frac{(1+z')dz'}{h(z')} \\ &= \frac{\Delta E'/(1+z)}{H_0 E_{\text{QG}}} \int_0^z \frac{(1+z')dz'}{h(z')}, \end{aligned} \quad (6)$$

where $\Delta E' = 100$ keV is the rest-frame energy difference. Similar to Ellis et al. [18], one can formulate the intrinsic

¹Due to the redshift dependence of cosmological sources, observer frame quantities can be quite different than source frame ones. In principle, there is a similar problem associated with the energy dependence of the observer-frame quantities for vacuum birefringence or WEP bounds (more on this below) when analyzing a large sample of cosmological sources with different redshifts. However, note that if we work on the observer-frame quantities of individual cosmological sources, there is no such a problem.

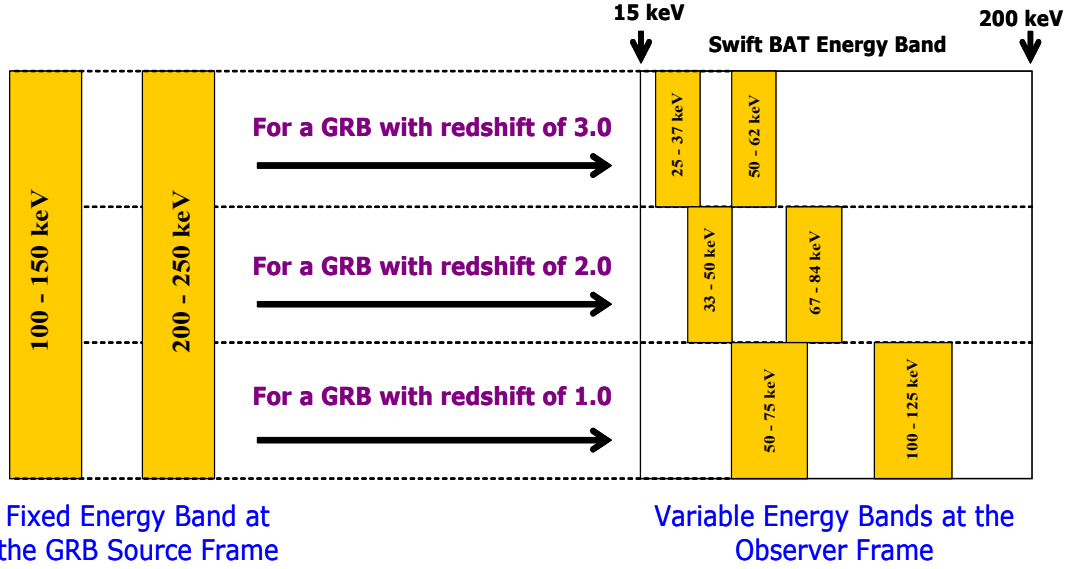


Fig. 2 Fixed energy bands in the GRB source frame are transformed to various energy bands in the observer frame, depending on the redshift. Reproduced from Ref. [123].

time lag problem in terms of linear regression:

$$\frac{\Delta t_{\text{src}}}{1+z} = a'_{\text{LV}} K' + b_{\text{sf}}, \quad (7)$$

where Δt_{src} is the extracted spectral lag for the source-frame energy bands 100–150 and 200–250 keV,

$$K' = \frac{1}{(1+z)^2} \int_0^z \frac{(1+z') dz'}{h(z')} \quad (8)$$

is a dimensionless redshift function, and $a'_{\text{LV}} = \Delta E'/(H_0 E_{\text{QG}})$ is the slope in K' . Using the sample of 56 GRBs with known redshifts, Wei & Wu [31] obtained robust limits on the slope a'_{LV} and the intercept b_{sf} by fitting their source-frame spectral lag data. The 95% confidence-level lower limit on the QG energy scale derived from a'_{LV} is $E_{\text{QG}} \geq 2.0 \times 10^{14}$ GeV [31]. This is a step forward in the study of LIV effects, since all previous investigations used spectral lags extracted in the observer frame only.

The second limitation of Ellis et al. treatment is that an unknown constant was supposed to be the intrinsic time delay in the linear fitting function (see Eq. 4), which is tantamount to suggesting that all GRBs have the same intrinsic time lag. However, since the time durations of GRBs span nearly six orders of magnitude, it is not possible that high-energy photons radiated from different GRBs (or from the same burst) have the same intrinsic time lag relative to the radiation time of low-energy photons [125]. As an improvement, Zhang & Ma [28] fitted the data of the high-energy photons from GRBs on several straight lines with the same slope as $1/E_{\text{QG},n}^n$ but with different intercepts (i.e., different intrinsic emission

times; see also Refs. [114–116]). However, photons from different GRBs fall on the same line, which still implies that the intrinsic time lags between the high-energy photons and the low-energy (trigger) photons are much the same for these GRBs. Chang et al. [23] made use of the magnetic jet model to estimate the intrinsic emission time delay between high- and low-energy photons from GRBs. However, the magnetic jet model depends on some specific theoretical parameters, and thus introduces uncertainties on the LIV results. In 2017, Wei et al. [29] first proposed that GRB 160625B, the burst having a well-defined transition from positive to negative spectral lags (see Figure 3), provides a good opportunity not only to disentangle the intrinsic time lag problem but also to put new constraints on LIV. The spectral lag is conventionally defined positive when high-energy photons arrive earlier than low-energy photons, while a negative lag corresponds to a delayed arrival of high-energy photons. As discussed above, the LIV-induced time delay Δt_{LIV} is likely to be accompanied by a potential intrinsic energy-dependent time lag Δt_{int} due to unknown properties of the source. Therefore, the observed time lag between two different energy bands of a GRB should consist of two parts,

$$\Delta t_{\text{obs}} = \Delta t_{\text{int}} + \Delta t_{\text{LIV}}. \quad (9)$$

Since the observed time lags of most GRBs have a positive energy dependence (e.g., Refs. [126, 127]), Wei et al. [29] approximated the observer-frame relation of the intrinsic time lag and the energy E as a power law with

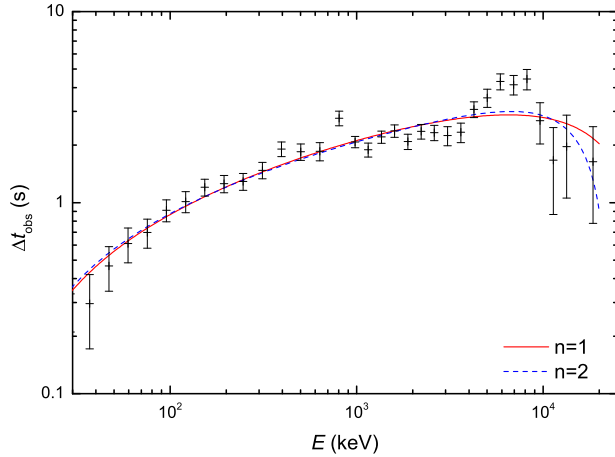


Fig. 3 Energy dependence of the observed time lag Δt_{obs} between the lowest-energy band and any other high-energy bands of GRB 160625B. The solid and dashed curves correspond to the best-fit linear ($n = 1$) and quadratic ($n = 2$) LIV models, respectively. Reproduced from Ref. [29].

positive dependence,

$$\Delta t_{\text{int}}(E) = \tau \left[\left(\frac{E}{\text{keV}} \right)^\alpha - \left(\frac{E_0}{\text{keV}} \right)^\alpha \right] \text{ s}, \quad (10)$$

where $\tau > 0$ and $\alpha > 0$, and where $E_0 = 11.34$ keV is the median value of the lowest reference energy band (10–12 keV). We emphasize that the intrinsic positive time lag implies an earlier arrival time for the higher energy photons. Also, when the subluminal case ($s_{\pm} = +1$) is considered, high-energy photons would arrive on Earth after low-energy ones, implying a negative spectral lag due to the LIV effects. As the Lorentz-violating term becomes dominant at higher energy scales, the positive correlation between the time lag and the energy would gradually trend in an opposite way. The combined contributions from the intrinsic time lag and the LIV-induced time lag can therefore produce the observed lag behavior with a turnover from positive to negative lags [29]. By fitting the spectral lag behavior of GRB 160625B, Wei et al. [29, 30] obtained both a reasonable formulation of the intrinsic energy-dependent time lag and comparatively robust limits on the QG energy scale and the coefficients of the Standard Model Extension. The 1σ confidence-level lower limits are $E_{\text{QG},1} > 0.5 \times 10^{16}$ GeV and $E_{\text{QG},2} > 1.4 \times 10^7$ GeV for linear and quadratic LIV, respectively. The spectral lag data of GRB 160625B does not have the current best sensitivity to LIV constraints, but the analysis method, when applied to future bright short GRBs with similar spectral-lag transitions, may result in more stringent constraints on LIV.

- Active galactic nuclei

Thanks to their fast flux variations (hours to years),

cosmological distances, and very high energy (VHE, $E \geq 100$ GeV) gamma-rays, TeV flares of AGNs have also been viewed as very effective probes for searching for the LIV-induced vacuum dispersions. It is worth pointing out that testing LIV with both GRBs and flaring AGNs is of great fundamental interest. GRBs can be detected at very large distances (up to $z \sim 8$), but with very limited high-energy ($E > \text{tens of GeV}$) photons. On the contrary, AGN flares can be well observed with large statistics of photons up to a few tens of TeV. But due to extinction of high-energy photons by extragalactic background light, TeV detections are limited to those sources with relatively low redshifts $z \leq 0.5$. Hence, GRBs and flaring AGNs are mutually complementary in testing LIV, and they allow to test different redshift and energy ranges. There have been some resulting constraints on LIV using TeV observations of bright AGN flares, including the Whipple analysis of the flare of Mrk 421 [34], the MAGIC and H.E.S.S. analyses of the flares of Mrk 501 [128–130], and the H.E.S.S. analysis of the flare of PKS 2155-304 [131, 132]. The current best limit for the linear case considering a subluminal LIV effect obtained with AGNs is from the H.E.S.S. analysis of the PKS 2155-304 flare data, namely $E_{\text{QG},1} > 2.1 \times 10^{18}$ GeV [132]. For the quadratic LIV, the best limits derived from AGNs have been set by H.E.S.S.’s observation of the TeV flare of Mrk 501. The reported limits are $E_{\text{QG},2} > 8.5 \times 10^{10}$ GeV ($E_{\text{QG},2} > 7.3 \times 10^{10}$ GeV) for the subluminal (superluminal) case [130].

- Pulsars

A third class of astrophysical sources used for the time-of-flight tests on gamma-rays are pulsars. When it comes to testing the quadratic LIV term, having a VHE emission will compensate for a short of distance. Gamma-ray pulsars, albeit being detected many orders of magnitude closer than GRBs or AGNs, have the advantage of precisely periodic flux variation, as well as the fact that they are the only stable candidate astrophysical sources for such time-of-flight studies. Sensitivity to LIV can therefore be improved by simply observing longer. Additionally, since the timing of the pulsar is carefully studied throughout the electromagnetic spectrum, energy-dependent time delays induced by propagation effects can be more easily distinguished from intrinsic delays. First limits on LIV using gamma-ray radiation from the galactic Crab pulsar were obtained from the observation of the Energetic Gamma-Ray Experiment Telescope (EGRET) onboard the Compton Gamma-Ray Observatory (CGRO) at energies above 2 GeV [35], and improved by the VERITAS data above 120 GeV [133, 134]. Recently, the MAGIC collaboration presented the best limits derived from pulsars by studying the Crab pulsar emission observed up to TeV energies, yielding $E_{\text{QG},1} >$

Table 1 A selection of lower limits on $E_{\text{QG},n}$ for linear ($n = 1$) and quadratic ($n = 2$) LIV for the subluminal ($s_{\pm} = +1$) and superluminal ($s_{\pm} = -1$) cases. These limits were obtained from vacuum dispersion time-of-flight measurements of various astrophysical sources.

Source(s)	Instrument	Technique	$E_{\text{QG},1}$ (GeV)		$E_{\text{QG},2}$ (GeV)		Refs.
			$s_{\pm} = +1$	$s_{\pm} = -1$	$s_{\pm} = +1$	$s_{\pm} = -1$	
9 GRBs ^a	BATSE+OSSE	Wavelets	6.9×10^{15}	—	2.9×10^6	—	[107]
GRB 021206 ^b	RHESSI	Peak times at different energies	1.8×10^{17}	—	—	—	[108]
35 GRBs ^c	BATSE+HETE-2+Swift	Wavelets	1.4×10^{16}	—	—	—	[18, 106]
GRB 051221A	Konus-Wind+Swift	Peak times of the light curves in different energy bands	6.6×10^{16}	—	6.2×10^6	—	[109]
15 GRBs	HETE-2	Wavelets	2.0×10^{15}	—	—	—	[110]
11 GRBs	INTEGRAL	Likelihood	3.2×10^{11}	—	—	—	[111]
GRB 080916C	Fermi GBM+LAT	Associating a 13.2 GeV photon with the trigger time	1.3×10^{18}	—	—	—	[21]
GRB 090510	Fermi GBM+LAT	Associating a 31 GeV photon with the start of the first GBM pulse	1.5×10^{19}	—	—	—	[22]
	Fermi/LAT	PairView+Likelihood+Sharpness-Maximization Method	9.3×10^{19}	1.3×10^{20}	1.3×10^{11}	9.4×10^{10}	[25]
GRB 160625B	Fermi/GBM	Spectral lag transition	0.5×10^{16}	—	1.4×10^7	—	[29]
56 GRBs	Swift	Rest-frame spectral lags	2.0×10^{14}	—	—	—	[31]
GRB 190114C	MAGIC	Likelihood	5.8×10^{18}	5.5×10^{18}	6.3×10^{10}	5.6×10^{10}	[33]
Mrk 421	Whipple	Binning	4.0×10^{16}	—	—	—	[34]
Mrk 501	MAGIC	Energy cost function	2.1×10^{17}	—	2.6×10^{10}	—	[128]
		Likelihood	3.0×10^{17}	—	5.7×10^{10}	—	[129]
	H.E.S.S.	Likelihood	3.6×10^{17}	2.6×10^{17}	8.5×10^{10}	7.3×10^{10}	[130]
PKS 2155-304	H.E.S.S.	Modified cross correlation function	7.2×10^{17}	—	1.4×10^9	—	[131]
		Likelihood	2.1×10^{18}	—	6.4×10^{10}	—	[132]
Crab pulsar	CGRO/EGRET	Pulse arrival times in different energy bands	1.8×10^{15}	—	—	—	[35]
	VERITAS	Likelihood	3.0×10^{17}	—	7.0×10^9	—	[133]
		Dispersion Cancellation	1.9×10^{17}	1.7×10^{17}	—	—	[134]
	MAGIC	Likelihood	5.5×10^{17}	4.5×10^{17}	5.9×10^{10}	5.3×10^{10}	[135]

^aLimits obtained not taking into account the factor $(1+z)$ in the intergrand of Eq. (3).

^bThe pseudo redshift was estimated from the spectral and temporal properties of GRB 021206.

^cThe Limits of Ellis et al. [18] were corrected in Ellis et al. [106] taking into account the factor $(1+z)$ in the intergrand of Eq. (3).

5.5×10^{17} GeV ($E_{\text{QG},1} > 4.5 \times 10^{17}$ GeV) for a linear, and $E_{\text{QG},2} > 5.9 \times 10^{10}$ GeV ($E_{\text{QG},2} > 5.3 \times 10^{10}$ GeV) for a quadratic LIV, for the subluminal (superluminal) case, respectively [135].

The most important constraints obtained so far with vacuum dispersion time-of-flight measurements of various astrophysical sources are summarized in Table 1. The most stringent lower limits to date on the linear and quadratic LIV energy scales were set by the observation of GRB 090510 with Fermi/LAT. The values for the subluminal (superluminal) case are $E_{\text{QG},1} > 9.3 \times 10^{19}$ GeV ($E_{\text{QG},1} > 1.3 \times 10^{20}$ GeV) and $E_{\text{QG},2} > 1.3 \times 10^{11}$ GeV ($E_{\text{QG},2} > 9.4 \times 10^{10}$ GeV) [25]. Clearly, these vacuum dispersion studies using gamma rays in the GeV–TeV range offer us at present with the best opportunity to search for Planck-scale modifications of the dispersion relation. Unfortunately, while they provide meaningful bounds for the linear ($n = 1$) modification, they are much weaker for deviations that arise at the quadratic ($n = 2$) order.

2.2 Vacuum birefringence from LIV

2.2.1 General formulae

In QG theories that invoke LIV, the Charge-Parity-Time (CPT) theorem, i.e., the invariance of the laws of physics under charge conjugation, parity transformation, and time reversal, no longer holds. Note that the fact CPT does not hold does not imply that it should be violated. In the absence of Lorentz invariance, the CPT invariance, if needed, should be imposed as an additional assumption. In the effective field theory approach [136], the Lorentz- and CPT-violating dispersion relation for photon propagation can be parameterized as

$$E_{\pm}^2 = p^2 c^2 \pm \frac{2\eta}{E_{\text{pl}}} p^3 c^3, \quad (11)$$

where \pm represents the left- or right-handed circular polarization states of the photon, and η is a dimensionless parameter that needs to be constrained. In LIV but CPT invariant theories, the parameter η exactly vanishes. In this sense, such tests might be less general than the ones based on vacuum dispersion. The linear polarization can be decomposed into left- and right-handed circular polarization states. For $\eta \neq 0$, photons with opposite circular polarizations have slightly different group velocities, which leads to a rotation of the polarization vector of a

linearly polarized wave. This effect is known as vacuum birefringence. The rotation angle propagating from the source at redshift z to the observer can be derived as [47, 49]

$$\Delta\phi_{\text{LIV}}(E) \simeq \eta \frac{E^2 F(z)}{\hbar E_{\text{pl}} H_0}, \quad (12)$$

where E is the observed photon energy, and

$$F(z) = \int_0^z \frac{(1+z') dz'}{\sqrt{\Omega_m (1+z')^3 + \Omega_\Lambda}}. \quad (13)$$

Generally speaking, it is impossible to know the intrinsic polarization angles in the emission of photons of different energies from a given source. If one had this information, evidence for vacuum birefringence (i.e., an energy-dependent rotation of the polarization plane) can be examined by measuring differences between the known intrinsic polarization angle and the observed polarization angles at different energies. However, even without such knowledge, the birefringent effect can still be constrained for polarized sources at arbitrary cosmological distances, because the differential rotation acting on the polarization angle as a function of energy would add opposite oriented polarization vectors, effectively erasing most, if not all, of the observed polarization signal. Therefore, the detection of the polarization signal can put an upper bound on such a possible violation.

2.2.2 Present constraints

Observations of linear polarization from distant sources have been widely used to place upper limits on the birefringent parameter η . The vacuum birefringence constraints arise from the fact if the rotation angle (Eq. 12) differs by more than $\pi/2$ over an energy range ($E_1 < E < E_2$), then the net polarization of the signal would be severely suppressed and well below any observed value. Hence, the measurement of polarization in a given energy band implies that the differential rotation angle $|\Delta\phi(E_2) - \Delta\phi(E_1)|$ should not be larger than $\pi/2$.

Previously, Gleiser & Kozameh [38] set an upper bound of $\eta < 10^{-4}$ by analyzing the linearly polarized ultraviolet light from the distant radio galaxy 3C 256. Much more stringent limits, $\eta < 10^{-14}$, have been obtained by using the linear polarization detection in the gamma-ray emission of GRB 021206 [43, 44]. However, the originally reported detection of high polarization from GRB 021206 [137] has been refuted by the re-analyses of the same data [138, 139]. Maccione et al. [140] used the hard X-ray polarization measurement of the Crab Nebula to get a constraint of $\eta < 9 \times 10^{-10}$. Laurent et al. [47] used a report of polarized soft gamma-ray emission from GRB 041219A to derive a stronger limit of $\eta < 1.1 \times 10^{-14}$ (see also Ref. [48]). But again,

this claimed polarization detection [141–143] has been disputed (see the explanations in Ref. [49]). That is, the previous reports of the gamma-ray polarimetry for GRB 041219A are controversial and, thus, the arguments for the limits on η given by Refs. [47, 48] are still open to questions.

Contrary to those disputed reports, the evidences of linearly polarized gamma-ray emission detected by the gamma-ray burst polarimeter (GAP) onboard the Interplanetary Kite-craft Accelerated by Radiation Of the Sun (IKAROS) are convincing, and thus these detections can be used to set more reliable limits on the birefringent parameter [49]. IKAROS/GAP detected gamma-ray polarizations of three GRBs with high significance levels, with a linear polarization degree of $\Pi = 27 \pm 11\%$ for GRB 100826A [144], $\Pi = 70 \pm 22\%$ for GRB 110301A, and $\Pi = 84^{+16}_{-28}\%$ for GRB 110721A [145]. The detection significance are 2.9σ , 3.7σ , and 3.3σ , respectively. Toma et al. [49] set the upper limit of the differential rotation angle $|\Delta\phi(E_2) - \Delta\phi(E_1)|$ to be $\pi/2$, and obtained a severe upper limit on η in the order of $\mathcal{O}(10^{-15})$ from the reliable polarimetric data of these three GRBs. However, the GRBs had no direct redshift measurement, they used a redshift estimate based on an empirical luminosity relation. Utilizing the real redshift measurement ($z = 1.33$) together with the polarization data of GRB 061122, Götz et al. [50] obtained a stricter limit ($\eta < 3.4 \times 10^{-16}$) on a possible LIV. Götz et al. [51] used the most distant polarized burst (up to $z = 2.739$), GRB 140206A, to obtain the deepest limit to date ($\eta < 1.0 \times 10^{-16}$) on the possibility of LIV.

It is worth noting that most of previous polarization constraints were derived under the assumption that the differential rotation angle $|\Delta\phi(E_2) - \Delta\phi(E_1)|$ is smaller than $\pi/2$. However, Lin et al. [52] gave a detailed analysis on the evolution of GRB polarization arising from the vacuum birefringent effect, and showed that a considerable amount of the initial polarization degree (depending both on the photon energy band and the photon spectrum) can be conserved even if $|\Delta\phi(E_2) - \Delta\phi(E_1)|$ is approaching to $\pi/2$. This is incompatible with the common belief that $|\Delta\phi(E_2) - \Delta\phi(E_1)|$ should not be too large when high polarization is detected. Therefore, Lin et al. [52] suggested that it is unsuitable to constrain the birefringent effect by simply setting $\pi/2$ as the upper limit of $|\Delta\phi(E_2) - \Delta\phi(E_1)|$. Lin et al. [52] applied their formulae for the polarization evolution to some true GRB events, and obtained the most stringent upper limit to date on the birefringent parameter from the polarimetric data of GRB 061122, i.e., $\eta < 0.5 \times 10^{-16}$. Following the analysis method presented in Ref. [52] and utilizing the recent measurements of gamma-ray linear polarization of GRBs, Wei [55] updated constraints on a possible LIV through the vacuum birefringent effect, and thereby im-

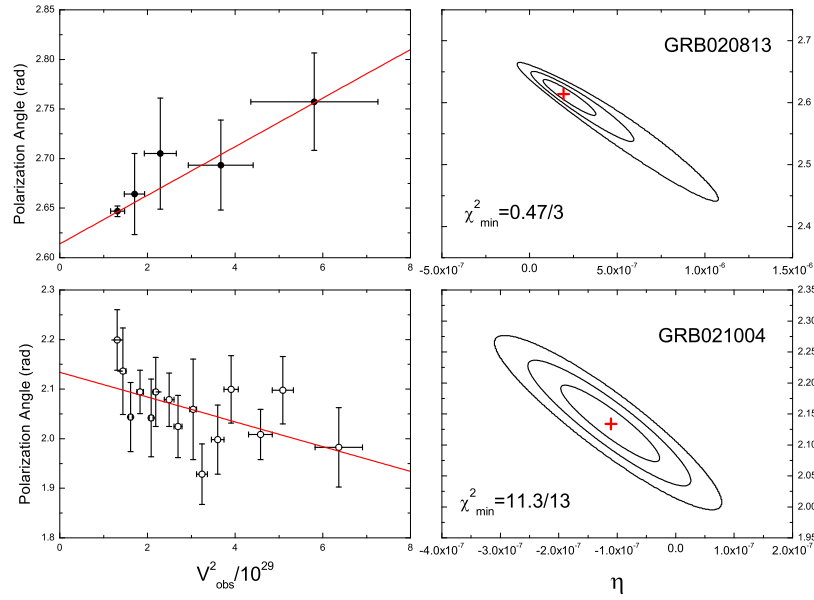


Fig. 4 Fit to the multiwavelength polarimetric data of the optical afterglows of GRB 020813 and GRB 021004. Left panels: linear fits of the observed linear polarization angles versus quantities of frequency squared. Right panels: 1-3 σ confidence levels in the ϕ_0 - η plane. Reproduced from Ref. [45].

proving previous results by factors ranging from two to ten.

If both the intrinsic polarization angle ϕ_0 and the rotation angle induced by the birefringent effect $\Delta\phi_{\text{LIV}}(E)$ are considered here, the observed linear polarization angle at a certain E from a source should be

$$\phi_{\text{obs}} = \phi_0 + \Delta\phi_{\text{LIV}}(E). \quad (14)$$

Assuming that all photons in the observed energy band-pass are emitted with the same (unknown) intrinsic polarization angle, we then expect to observe the birefringent effect as an energy-dependent linear polarization vector. To constrain the birefringent parameter η , Fan et al. [45] looked for a similar energy-dependent trend in the multiwavelength polarization observations of the optical afterglows of GRB 020813 and GRB 021004. By fitting the spectropolarimetric data of these two GRBs, Fan et al. [45] obtained constraints on both ϕ_0 and η (see Figure 4). At the 3 σ confidence level, the combined limit on η from two GRBs is $-2 \times 10^{-7} < \eta < 1.4 \times 10^{-7}$. It is clear from Eq. (12) that the higher energy band of the polarization observation and the larger distance of the polarized source, the greater sensitivity to small values of η . As expected, the optical polarization data of GRB afterglow obtained a less stringent constraint on η [45].

2.2.3 Comparison with time-of-flight limits

Table 2 presents a summary of the corresponding limits on LIV from the polarization measurements of astro-

physical sources. The hitherto most stringent constraints on the birefringent parameter, $\eta < \mathcal{O}(10^{-16})$, have been obtained by the detections of linear polarization in the prompt gamma-ray emission of GRBs [50–52, 55].

By comparing Eqs. (1) and (11), we can derive the conversion from η to the Limit on the linear LIV energy scale, i.e., $E_{\text{QG},1} = \frac{E_{\text{pl}}}{2\eta}$. With the data presented in Tables 1 and 2, it is easy to compare the recent achievements in sensitivity of time-of-flight measurements versus polarization measurements. For the subluminal case, the time-of-flight analysis of multi-GeV photons from GRB 090510A detected by Fermi/LAT yielded the strictest limit on the linear LIV energy scale, $E_{\text{QG},1} > 9.3 \times 10^{19}$ GeV, which corresponds to $\eta < 0.07$ [25]. Obviously, this time-of-flight constraint is many orders of magnitude weaker than the best polarization constraint. However, time-of-flight constraints are essential in a broad-based search for nonbirefringent Lorentz-violating effects.

3 Astrophysical bounds on the photon mass

3.1 Dispersion from a nonzero photon mass

For a nonzero photon rest mass ($m_\gamma \neq 0$), the energy of the photon can be written as

$$E = \sqrt{p^2 c^2 + m_\gamma^2 c^4}. \quad (15)$$

Table 2 A selection of limits on the vacuum birefringent parameter η from the linear polarization measurements of astrophysical sources.

Author (year)	Source	Polarimeter	Energy band ^a	Π	η	Refs.
Gleiser and Kozameh (2001)	3C 256	Spectropolarimeter	Ultraviolet	$16.4 \pm 2.2\%$	$< 10^{-4}$	[38]
Mitrofanov (2003)	GRB 021206 ^c	RHESSI	150–2000 keV	$80 \pm 20\%^b$	$< 10^{-14}$	[43]
Jacobson et al. (2004)	GRB 021206 ^d	RHESSI	150–2000 keV	$80 \pm 20\%^b$	$< 0.5 \times 10^{-14}$	[44]
Fan et al. (2007)	GRB 020813	LRISp	3500–8800 Å	1.8%–2.4%	$(-2.0-1.4) \times 10^{-7}$	[45]
	GRB 021004	VLT	3500–8600 Å	$1.88 \pm 0.05\%$	$(-2.0-1.4) \times 10^{-7}$	
Maccione et al. (2008)	Crab Nebula	INTEGRAL/SPI	100–1000 keV	$46 \pm 10\%$	$< 9 \times 10^{-10}$	[140]
Laurent et al. (2011)	GRB 041219A ^e	INTEGRAL/IBIS	200–800 keV	$43 \pm 25\%^b$	$< 1.1 \times 10^{-14}$	[47]
Stecker (2011)	GRB 041219A ^f	INTEGRAL/SPI	100–350 keV	$96 \pm 40\%^b$	$< 2.4 \times 10^{-15}$	[48]
Toma et al. (2012)	GRB 100826A ^f	IKAROS/GAP	70–300 keV	$27 \pm 11\%$	$< 2.0 \times 10^{-14}$	[49]
	GRB 110301A ^f	IKAROS/GAP	70–300 keV	$70 \pm 22\%$	$< 1.0 \times 10^{-14}$	
	GRB 110721A ^f	IKAROS/GAP	70–300 keV	$84^{+16}_{-28}\%$	$< 2.0 \times 10^{-15}$	
Götz et al. (2013)	GRB 061122	INTEGRAL/IBIS	250–800 keV	$> 60\%$	$< 3.4 \times 10^{-16}$	[50]
Götz et al. (2014)	GRB 140206A	INTEGRAL/IBIS	200–400 keV	$> 48\%$	$< 1.0 \times 10^{-16}$	[51]
Lin et al. (2016)	GRB 061122	INTEGRAL/IBIS	250–800 keV	$> 60\%$	$< 0.5 \times 10^{-16}$	[52]
	GRB 110721A ^f	IKAROS/GAP	70–300 keV	$84^{+16}_{-28}\%$	$< 4.0 \times 10^{-16}$	
Wei (2019)	GRB 061122	INTEGRAL/IBIS	250–800 keV	$> 60\%$	$< 0.5 \times 10^{-16}$	[55]
	GRB 100826A ^f	IKAROS/GAP	70–300 keV	$27 \pm 11\%$	$1.2^{+1.4}_{-0.7} \times 10^{-14}$	
	GRB 110301A ^f	IKAROS/GAP	70–300 keV	$70 \pm 22\%$	$4.3^{+5.4}_{-2.3} \times 10^{-15}$	
	GRB 110721A	IKAROS/GAP	70–300 keV	$84^{+16}_{-28}\%$	$5.1^{+4.0}_{-5.1} \times 10^{-16}$	
	GRB 140206A	INTEGRAL/IBIS	200–400 keV	$> 48\%$	$< 1.0 \times 10^{-16}$	
	GRB 160106A ^f	AstroSat/CZTI	100–300 keV	$68.5 \pm 24\%$	$3.4^{+1.4}_{-1.8} \times 10^{-15}$	
	GRB 160131A	AstroSat/CZTI	100–300 keV	$94 \pm 31\%$	$1.2^{+2.0}_{-1.2} \times 10^{-16}$	
	GRB 160325A ^f	AstroSat/CZTI	100–300 keV	$58.75 \pm 23.5\%$	$2.3^{+1.0}_{-0.9} \times 10^{-15}$	
	GRB 160509A	AstroSat/CZTI	100–300 keV	$96 \pm 40\%$	$0.8^{+2.2}_{-0.8} \times 10^{-16}$	
	GRB 160802A ^f	AstroSat/CZTI	100–300 keV	$85 \pm 29\%$	$2.0^{+1.7}_{-2.0} \times 10^{-15}$	
	GRB 160821A ^f	AstroSat/CZTI	100–300 keV	$48.7 \pm 14.6\%$	$8.9^{+1.7}_{-1.7} \times 10^{-15}$	
	GRB 160910A ^f	AstroSat/CZTI	100–300 keV	$93.7 \pm 30.92\%$	$4.7^{+7.6}_{-4.7} \times 10^{-16}$	

^aThe energy band in which polarization is observed.

^bThe claimed polarization detections have been refuted.

^cThe distance of GRB 021206 was taken to be 10^{10} light years.

^dThe distance of GRB 021206 was taken to be 0.5 Gpc.

^eThe lower limit to the photometric redshift of GRB 041219A ($z = 0.02$) was adopted.

^fThe redshifts of these GRBs were estimated by the empirical luminosity relation.

Then the massive photon group velocity v in vacuum is no longer a constant c , but depends on the photon frequency ν . That is,

$$v = \frac{\partial E}{\partial p} = c \sqrt{1 - \frac{m_\gamma^2 c^4}{E^2}} \approx c \left(1 - \frac{1}{2} \frac{m_\gamma^2 c^4}{h^2 \nu^2} \right), \quad (16)$$

where the last approximation is valid when $m_\gamma \ll h\nu/c^2 \simeq 7 \times 10^{-42} (\frac{\nu}{\text{GHz}})$ kg. Eq. (16) implies that the lower frequency, the slower the photon travels in vacuum. Two massive photons with different frequencies ($\nu_l < \nu_h$), if emitted simultaneously from a same source, would be received at different times by the observer. For a cosmic source, the arrival time difference due to a nonzero photon mass is given by

$$\Delta t_{m_\gamma} = \frac{m_\gamma^2 c^4}{2h^2 H_0} (\nu_l^{-2} - \nu_h^{-2}) H_\gamma(z), \quad (17)$$

where $H_\gamma(z)$ is a dimensionless function of the source redshift z ,

$$H_\gamma(z) = \int_0^z \frac{(1+z')^{-2} dz'}{\sqrt{\Omega_m(1+z')^3 + \Omega_\Lambda}}. \quad (18)$$

It is obvious from Eq. (17) that observations of shorter time structures at lower frequencies from sources at cosmological distances are particularly powerful for constraining the photon mass. In contrast, observations of high-energy photons from cosmological sources are better suited for probing LIV [16].

The observed time delays between different energy bands from astrophysical sources have been used to constrain the photon mass. For instance, Lovell et al. [61] analysed the delay between the optical and radio emission from flare stars and concluded that the relative velocity of light and radio waves was constrained to be 4×10^{-7} over a wavelength range from $0.54 \mu\text{m}$ to 1.2 m , which implied an upper limit on the photon mass of $m_\gamma \leq 1.6 \times 10^{-45} \text{ kg}$. With the arrival time delay of optical pulses from the Crab Nebula pulsar over a wavelength range of $0.35\text{--}0.55 \mu\text{m}$, Warner & Nather [62] set a stringent limit on the possible frequency-dependence of the speed of light, which led to an upper limit of $m_\gamma \leq 5.2 \times 10^{-44} \text{ kg}$. By analyzing the arrival time delay between the radio afterglow and the prompt gamma-ray emission from GRB 980703, Schaefer [63] obtained a stricter upper limit of $m_\gamma \leq 4.2 \times 10^{-47} \text{ kg}$. Using GRB early-time radio detections as well as multi-band radio afterglow peaks, Zhang et al. [64] improved the results of Schaefer [63] by nearly half an order of magnitude. Although the optical emissions of the Crab Nebula pulsar have been used to constrain the photon mass, Wei et al. [65] showed that much more severe limits on the photon mass can be obtained with radio observations of

pulsars in the Large and Small Magellanic Clouds (LMC and SMC). The photon mass limits can be as low as $m_\gamma \leq 2.0 \times 10^{-48} \text{ kg}$ for the radio pulsar PSR J0451-67 in the LMC and $m_\gamma \leq 2.3 \times 10^{-48} \text{ kg}$ for PSR J0045-7042 in the SMC [65]. Owing to their fine time structures, low frequency emissions, and large cosmological distances, extragalactic fast radio bursts (FRBs) have been viewed as the most promising celestial laboratory so far for testing the photon mass [66–69, 71, 72]. The first attempts to constrain the photon mass using FRBs were presented in Wu et al. [66] and Bonetti et al. [67]. Adopting the possible redshift $z = 0.492$ for FRB 150418, and assuming the dispersive delay was caused by the nonzero photon mass effect, Wu et al. [66] improved the limit of the photon mass to be $m_\gamma \leq 5.2 \times 10^{-50} \text{ kg}$ (see also [67]). However, the identification of a radio transient, which provided the redshift measurement to FRB 150418, was challenged with a common AGN variability [146, 147]. Now this redshift measurement is generally thought to be unreliable [148]. Subsequently, Bonetti et al. [68] used the confirmed redshift measurement of FRB 121102 to obtain a similar result of $m_\gamma \leq 3.9 \times 10^{-50} \text{ kg}$. After correcting for dispersive delay, Hessels et al. [149] found that the subbursts of FRB 121102 still show a time-frequency downward drifting pattern. The frequency-dependent time delay between subbursts is much smaller than the dispersive delay, resulting in a tighter upper limit on the photon mass of $m_\gamma \leq 5.1 \times 10^{-51} \text{ kg}$ [71]. The current astrophysical constraints on the photon rest mass derived through the dispersion method are shown in Figure 5. Most of these results were based on a single source, in which the observed time delay was assumed to be due to the nonzero photon mass and the dispersion from the plasma effect (see below) was ignored.

3.2 Dispersion from the plasma effect

Due to the dispersive nature of plasma, radio waves with lower frequencies would travel through the ionized medium slower than those with higher frequencies [150]. That is, the group velocity of electromagnetic waves propagating through a plasma has a frequency dependence, i.e.,

$$v_p = c \left[1 - \left(\frac{\nu_p}{\nu} \right)^2 \right]^{1/2}, \quad (19)$$

where the plasma frequency $\nu_p = [n_e e^2 / (4\pi^2 m_e \epsilon_0)]^{1/2}$ with n_e the average electron number density along the line of sight, e and m_e the charge and mass of an electron, respectively, and ϵ_0 the permittivity of vacuum. The arrival time delay between two wave packets with different frequencies, which caused by the plasma effect, can then

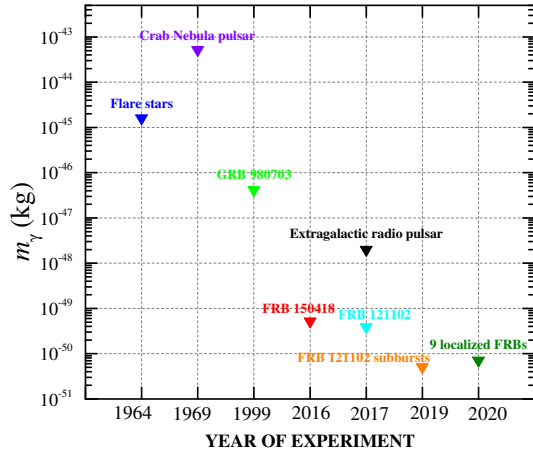


Fig. 5 Astrophysical limits on the photon rest mass through the dispersion method, including the strict upper bounds from flare stars [61], Crab nebula pulsar [62], GRB 980703 [63], extragalactic radio pulsar [65], FRB 150418 [66, 67], FRB 121102 [68], FRB 121102 subbursts [71], and nine localized FRBs [72].

be expressed as

$$\begin{aligned} \Delta t_{\text{DM}} &= \int \frac{dl}{c} \frac{\nu_p^2}{2} (\nu_l^{-2} - \nu_h^{-2}) \\ &= \frac{e^2}{8\pi^2 m_e \epsilon_0 c} (\nu_l^{-2} - \nu_h^{-2}) \text{DM}_{\text{astro}}. \end{aligned} \quad (20)$$

Here the dispersion measure (DM) is defined as the integrated electron number density along the propagation path, $\text{DM}_{\text{astro}} \equiv \int n_e dl$. In a cosmological context, the measured DM_{astro} by an earth observer is $\text{DM}_{\text{astro}} \equiv \int n_{e,z} (1+z)^{-1} dl$, where $n_{e,z}$ is the rest-frame number density of free electrons [151]. For a cosmological source at redshift z , we expect DM_{astro} to separate into four components:

$$\text{DM}_{\text{astro}} = \text{DM}_{\text{MW}} + \text{DM}_{\text{MW halo}} + \text{DM}_{\text{IGM}} + \frac{\text{DM}_{\text{host}}}{1+z} \quad (21)$$

with DM_{MW} the contribution from the Milky Way ionized interstellar medium, $\text{DM}_{\text{MW halo}}$ the contribution from the Milky Way halo, DM_{IGM} the contribution from the intergalactic medium (IGM), and DM_{host} the contribution from the host galaxy and source environment in the cosmological rest frame of the source. The measured value of DM_{host} is smaller by a factor of $(1+z)$ [151].

It is evident from Eq. (20) that radio waves propagating through a plasma are expected to arrive with a frequency-dependent dispersion in time of the $1/\nu^2$ behavior. However, a similar dispersion $\propto m_\gamma^2/\nu^2$ [see Eq. (17)] could also be caused by a nonzero photon mass. The dispersion method used for constraining the photon

mass is, therefore, hindered by the similar frequency dependences of the dispersions arise from the plasma and nonzero photon mass effects.

3.3 Combined limits on the photon mass

In order to diagnose an effect as radical as a finite photon mass, statistical and possible systematic uncertainties must be carefully handled. One can not rely solely on a single source, for which it would be hard to distinguish the dispersions from the plasma and photon mass. For this reason, Shao & Zhang [69] constructed a Bayesian framework to derive a combined constraint of $m_\gamma \leq 8.7 \times 10^{-51}$ kg from a sample of 21 FRBs (including 20 FRBs without measured redshift, and one, FRB 121102, with a known redshift), where an uninformative prior was used for the unknown redshift. Wei & Wu [70] also developed a statistical approach to study this problem by analyzing a catalog of radio sources with measured DMs. This technique has the advantage that it can both give a combined limit of the photon mass and estimate an average DM_{astro} contributed by the plasma effect. Using the measured DMs from two statistical samples of extragalactic radio pulsars, Wei & Wu [70] placed combined limits on the photon mass at 68% confidence level, i.e., $m_\gamma \leq 1.5 \times 10^{-48}$ kg for the sample of 22 LMC pulsars and $m_\gamma \leq 1.6 \times 10^{-48}$ kg for the other sample of 5 SMC pulsars.

Since the dispersions from the plasma and photon mass have different redshift dependences, Refs. [67, 68, 150] suggested that they could in principle be distinguished by a statistical sample of FRBs at a range of different redshifts, thereby improving the sensitivity to m_γ . Recently, nine FRBs with different redshift measurements (FRB 121102: $z = 0.19723$ [148, 152, 153]; FRB 180916.J0158+65: $z = 0.0337$ [154]; FRB 180924: $z = 0.3214$ [155]; FRB 181112: $z = 0.4755$ [156]; FRB 190523: $z = 0.66$ [157]; FRB 190102: $z = 0.291$; FRB 190608: $z = 0.1178$; FRB 190611: $z = 0.378$; FRB 190711: $z = 0.522$ [158]) have been reported. Wei & Wu [72] applied the idea suggested by Refs. [67, 68, 150] to these nine localized FRBs to give a combined constraint on the photon mass. From observations, the radio signals of all FRBs exhibit an apparent ν^{-2} -dependent time delay, which is expected from both the free electron content along the line of the sight and nonzero mass effects on photon propagation (see Eqs. 17 and 20). Thus, Wei & Wu [72] attributed the observed time delay to two terms:

$$\Delta t_{\text{obs}} = \Delta t_{\text{DM}} + \Delta t_{m_\gamma}. \quad (22)$$

In practice, the observed DM of each FRB, DM_{obs} , is directly determined by fitting the ν^{-2} behavior of its observed time delay. This implies that both the line-of-sight free electron density and a massive photon (if it

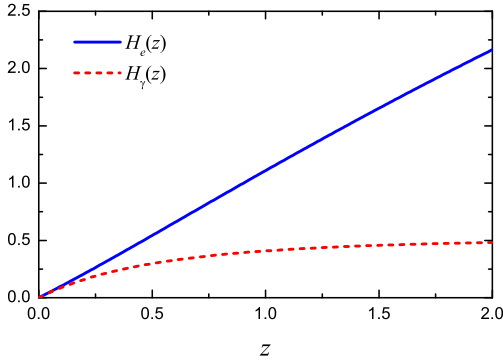


Fig. 6 Dependence of functions $H_\gamma(z)$ and $H_e(z)$ on the redshift z . Reproduced from Ref. [72].

exists) determine the same DM_{obs} , i.e.,

$$DM_{\text{obs}} = DM_{\text{astro}} + DM_\gamma, \quad (23)$$

where DM_{astro} is given in Eq. (21) and DM_γ denotes the “effective DM” due to a nonzero photon mass [69],

$$DM_\gamma \equiv \frac{4\pi^2 m_e \epsilon_0 c^5}{h^2 e^2} \frac{H_\gamma(z)}{H_0} m_\gamma^2. \quad (24)$$

To investigate the possible DM_γ , we need to figure out different DM contributions in Eq. (21). For a localized FRB, the DM_{MW} term can be well estimated from a model of our Galactic electron distribution. The DM_{MWhalo} term is not well modeled, but is expected to contribute about $50\text{--}80 \text{ pc cm}^{-3}$ [159]. Wei & Wu [72] adopted $DM_{\text{MWhalo}} = 50 \text{ pc cm}^{-3}$. The DM_{host} term is highly uncertain, due to the dependences on the type of the FRB host galaxy, the relative orientations of the galaxy disk and source, and the near-source plasma [160]. Wei & Wu [72] assumed that the rest-frame DM_{host} scales with the star formation rate (SFR; see Ref. [161] for more details), $DM_{\text{host}}(z) = DM_{\text{host},0} \sqrt{\text{SFR}(z)/\text{SFR}(0)}$, where $DM_{\text{host},0}$ represents the present value of $DM_{\text{host}}(z=0)$ and $\text{SFR}(z) = \frac{0.0157+0.118z}{1+(z/3.23)^{4.66}} M_\odot \text{ yr}^{-1} \text{ Mpc}^{-3}$ is the empirical form of the star formation history [162, 163]. In the analysis of Wei & Wu [72], $DM_{\text{host},0}$ was treated as a free parameter. The IGM contribution to the DM of an FRB at redshift z is related to the ionization fractions of hydrogen and helium in the universe. Since both hydrogen and helium are fully ionized at $z < 3$, one then has [151]

$$DM_{\text{IGM}}(z) = \frac{21cH_0\Omega_b f_{\text{IGM}}}{64\pi G m_p} H_e(z), \quad (25)$$

where m_p is the proton mass, $\Omega_b = 0.0493$ is the baryonic matter energy density [164], $f_{\text{IGM}} \simeq 0.83$ is the fraction of baryon mass in the IGM [165], and $H_e(z)$ is the dimensionless redshift function,

$$H_e(z) = \int_0^z \frac{(1+z')dz'}{\sqrt{\Omega_m(1+z')^3 + \Omega_\Lambda}}. \quad (26)$$

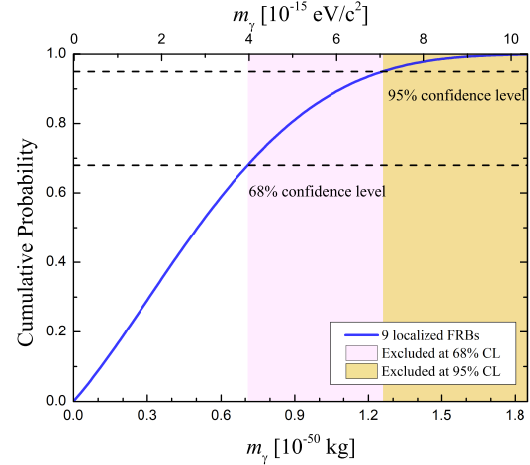


Fig. 7 Cumulative posterior probability distribution on the photon rest mass m_γ derived from nine localized FRBs. The excluded values for m_γ at 68% and 95% confidence levels are displayed with shadowed areas. Reproduced from Ref. [72].

The two dimensionless quantities (H_e and H_γ) as a function of the redshift z are displayed in Figure 6. One can see from this plot that the IGM and a possible photon mass contributions to DMs have different redshift dependences. As already commented, Bonetti et al. [67, 68] indicated that the different redshift dependences might not only be able to break dispersion degeneracy but also improve the sensitivity to m_γ at the point when a few redshift measurements of FRBs become available (see also Refs. [69, 150]).

With the redshift measurements of nine FRBs, Wei & Wu [72] maximized the likelihood function,

$$\mathcal{L} = \prod_i \frac{1}{\sqrt{2\pi}\sigma_{\text{tot},i}} \times \exp \left\{ -\frac{[DM_{\text{obs},i} - DM_{\text{astro},i} - DM_\gamma(m_\gamma, z_i)]^2}{2\sigma_{\text{tot},i}^2} \right\}, \quad (27)$$

to derive a combined limit on the photon mass m_γ . Here the total variance on each FRB is given by

$$\sigma_{\text{tot}}^2 = \sigma_{\text{obs}}^2 + \sigma_{\text{MW}}^2 + \sigma_{\text{MWhalo}}^2 + \sigma_{\text{int}}^2, \quad (28)$$

where σ_{obs} , σ_{MW} , and σ_{MWhalo} correspond to the uncertainties of DM_{obs} , DM_{MW} , and DM_{MWhalo} , respectively, and σ_{int} represents the global intrinsic scatter that might originate from the diversity of host galaxy contribution and the large IGM fluctuation. The marginalized cumulative posterior distribution of the photon mass m_γ is shown in Figure 7. The 68% confidence-level upper limit on m_γ from nine localized FRBs is $m_\gamma \leq 7.1 \times 10^{-51} \text{ kg}$ [72], which is comparable with or represents a factor of 7 improvement over existing photon mass limits from the individual FRBs [66–68, 71].

Table 3 Summary of astrophysical upper bounds on the photon rest mass as obtained by the dispersion method.

Author (year)	Source(s)	Wavelength (energy or frequency) range	m_γ (kg)	Refs.
Lovell et al. (1964)	flare stars	0.54 μm –1.2 m	1.6×10^{-45}	[61]
Warner and Nather (1969)	Crab Nebula pulsar	0.35–0.55 μm	5.2×10^{-44}	[62]
Schaefer (1999)	GRB 980703	5.0×10^9 – 1.2×10^{20} Hz	4.2×10^{-47}	[63]
Zhang et al. (2016)	GRB 050416A	8.46 GHz–15 keV	1.1×10^{-47}	[64]
Wei et al. (2017)	Extragalactic radio pulsar (PSR J0451-67)	~ 1.4 GHz	2.0×10^{-48}	[65]
	Extragalactic radio pulsar (PSR J0045-7042)	~ 1.4 GHz	2.3×10^{-48}	
Wei and Wu (2018)	22 radio pulsars in the LMC	~ 1.4 GHz	1.5×10^{-48}	[70]
	5 radio pulsars in the SMC	~ 1.4 GHz	1.6×10^{-48}	
Wu et al. (2016)	FRB 150418	1.2–1.5 GHz	5.2×10^{-50}	[66]
Bonetti et al. (2016)	FRB 150418	1.2–1.5 GHz	3.2×10^{-50}	[67]
Bonetti et al. (2017)	FRB 121102	1.1–1.7 GHz	3.9×10^{-50}	[68]
Shao and Zhang (2017)	21 FRBs (20 of them without redshift measurement)	\sim GHz	8.7×10^{-51}	[69]
Xing et al. (2019)	FRB 121102 subbursts	1.34–1.37 GHz	5.1×10^{-51}	[71]
Wei and Wu (2020)	9 localized FRBs	\sim GHz	7.1×10^{-51}	[72]

Table 3 presents a summary of astrophysical upper bounds on the photon mass m_γ obtained through the dispersion method. As illustrated in Figure 5 and Table 3, the current best m_γ limits were made by using the observations of FRB 121102 subbursts ($m_\gamma \leq 5.1 \times 10^{-51}$ kg) [71] and nine localized FRBs ($m_\gamma \leq 7.1 \times 10^{-51}$ kg) [72].

4 Astrophysical tests of the WEP

The WEP states that inertial and gravitational masses are identical. An alternative statement is that the trajectory of a freely falling, uncharged test body is independent of its internal structure and composition. Astrophysical observations provide a unique test of WEP by testing if different massless particles experience gravity differently. In this section, we present the field-standard test method through the Shapiro time delay effect.

Particles which traverse a gravitational field would experience a time delay (named the Shapiro delay) due to the warping of spacetime. Adopting the PPN formalism, the γ -dependent Shapiro delay is given by [95]

$$t_{\text{gra}} = -\frac{1+\gamma}{c^3} \int_{r_e}^{r_o} U(r) dr, \quad (29)$$

where r_e and r_o denote the locations of the emitting source and observer, respectively, and $U(r)$ is the gravitational potential along the propagation path. A possible violation of the WEP implies that, if two particles follow the same path through a gravitational potential, then they would undergo different Shapiro delays. In this case, two test particles emitted simultaneously from the source would reach our Earth with a arrival-time differ-

ence (see Figure 8)

$$\Delta t_{\text{gra}} = \frac{\Delta\gamma}{c^3} \int_{r_e}^{r_o} U(r) dr, \quad (30)$$

where $\Delta\gamma = |\gamma_2 - \gamma_1|$ represents the difference of the γ values for different particles, which can be used as measure of a possible deviation from the WEP.

To estimate the relative Shapiro delay Δt_{gra} with Eq. (30), one needs to figure out the gravitational potential $U(r)$. For sources at cosmological distances, $U(r)$ should have contributions from the local gravitational potential $U_{\text{local}}(r)$, the intergalactic potential $U_{\text{IG}}(r)$, and the host galaxy potential $U_{\text{host}}(r)$. Since the potential function for $U_{\text{IG}}(r)$ and $U_{\text{host}}(r)$ is hard to model, for the purposes of obtaining lower limits, it is reasonable to extend the local potential $U_{\text{local}}(r)$ to the distance of the source. In previous articles, the gravitational potential of the Milky Way, Virgo Cluster, or the Laniakea supercluster [166] has been adopted as the local potential, which can be modeled as a Keplerian potential $U(r) = -GM/r$. We thus have [96, 100]

$$\Delta t_{\text{gra}} = \Delta\gamma \frac{GM}{c^3} \times \ln \left\{ \frac{[d + (d^2 - b^2)^{1/2}][r_L + s_n(r_L^2 - b^2)^{1/2}]}{b^2} \right\}, \quad (31)$$

where M is the mass of the gravitational field source, d is the distance from the particle source to the center of gravitational field, b is the impact parameter of the particle paths relative to the center, r_L is the distance of the center, and $s_n = +1$ (or -1) corresponds to the case where the particle source is located in the same (or opposite) direction with respect to the center of gravitational

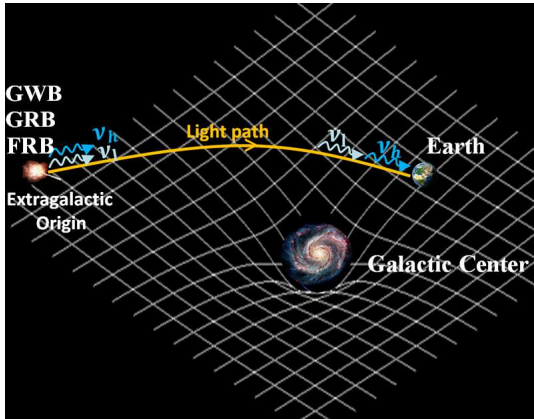


Fig. 8 A cartoon picture shows how two photons, one at a low frequency (ν_l) and another at a high frequency (ν_h), travel in curved space-time from their origin in a distant extragalactic transient until reaching our Earth. A lower-limit estimate of the gravitational pull that the photons experience along their way is given by the mass in the center of the Milky Way.

field. For a particle source at the coordinates (R.A.= β_s , Dec.= δ_s), the impact parameter b can be estimated as

$$b = r_G \sqrt{1 - (\sin \delta_s \sin \delta_L + \cos \delta_s \cos \delta_L \cos(\beta_s - \beta_L))^2}, \quad (32)$$

where β_L and δ_L represent the coordinates of the center of gravitational field.

4.1 Arrival time tests of the WEP

If one assumes that the observed time delay (Δt_{obs}) between messengers or within messengers is mainly contributed by the relative Shapiro delay (Δt_{gra}) and we know that the intrinsic (astrophysical) time delay $\Delta t_{\text{int}} > 0$, a conservative upper limit on the WEP violation could be placed by²

$$\Delta\gamma < \Delta t_{\text{obs}} \left(\frac{GM}{c^3} \right)^{-1} \times \ln^{-1} \left\{ \frac{\left[d + (d^2 - b^2)^{1/2} \right] \left[r_L + s_n (r_L^2 - b^2)^{1/2} \right]}{b^2} \right\} \quad (33)$$

The first multimessenger test of the WEP was between photons and neutrinos from supernova SN 1987A.

²Minazzoli et al. [167] discussed the shortcomings of standard Shapiro delay-based tests of the WEP. Because such tests are based on the estimation for different messenger particles of the one-way propagation time between the emitting source and the observer that is not an observable per se. As a consequence, Minazzoli et al. [167] suggested that such tests are extremely model dependent and can not provide reliable quantitative limits on the WEP violation.

Logo [97] and Krauss & Tremaine [96] used the observed time delay between photons and MeV neutrinos from SN 1987A to prove that the γ values for photons and neutrinos are identical to an accuracy of approximately 0.3–0.5%. These constraints can be further improved using the likely associations of high-energy neutrinos with the flaring blazars [168–171] or GRBs [172]. Besides the neutrino-photon sectors, the coincident detections of GW events with electromagnetic counterparts also provided multimessenger tests of the WEP, extending the WEP tests with GWs and photons [100, 173–180]. For example, with the assumption that the arrival time delay between GW170817 and GRB 170817A (~ 1.7 s) from a binary neutron star merger is mainly due to the gravitational potential of the Milky Way outside a sphere of 100 kpc, Abbott et al. [174] derived $-2.6 \times 10^{-7} \leq \gamma_g - \gamma_\gamma \leq 1.2 \times 10^{-6}$. A more severe constraint of $|\gamma_g - \gamma_\gamma| < 0.9 \times 10^{-10}$ can be achieved for GW170817/GRB 170817A when the gravitational potential of the Virgo Cluster is considered [177].

WEP tests have also been performed within the same species of messenger particles (neutrinos, photons, or GWs) but with varying energies (e.g., [71, 96, 98–100, 181–194]). In the neutrino sector, Longo [96] used the observed delay between 7.5 MeV and 40 MeV neutrinos from SN 1987A to set $|\gamma_\nu(40 \text{ MeV}) - \gamma_\nu(7.5 \text{ MeV})| < 1.6 \times 10^{-6}$. Wei et al. [171] adopted the delay for neutrinos ranging in energy from about 0.1 to 20 TeV from the direction of the blazar TXS 0506+056 to obtain $|\gamma_\nu(20 \text{ TeV}) - \gamma_\nu(0.1 \text{ TeV})| < 7.3 \times 10^{-6}$. In the photon sector, Gao et al. [98] (see also Sivaram [181]) suggested that one can use the time delays of photons of different energies from cosmological transients to test the WEP. They applied the similar approach to GRBs and derived $|\gamma_\gamma(\text{eV}) - \gamma_\gamma(\text{MeV})| < 1.2 \times 10^{-7}$ for GRB 080319B and $|\gamma_\gamma(\text{GeV}) - \gamma_\gamma(\text{MeV})| < 2.0 \times 10^{-8}$ for GRB 090510. Recently, such a test has also been applied to different-energy photons in other transient sources, including FRBs [71, 99, 185–187], TeV blazars [188], and the Crab pulsar [189–192]. In the GW sector, Wu et al. [100] suggested that one can treat the GW signals with different frequencies as different gravitons to test the WEP. They used the delay for the GW signals ranging in frequency from about 35 to 150 Hz from GW150914 to set $|\gamma_g(35 \text{ Hz}) - \gamma_g(150 \text{ Hz})| < 10^{-9}$ (see also [193]). Very recently, Yang et al. [194] obtained new constraints of $\Delta\gamma$ by using the GW data of binary black holes mergers in the LIGO-Virgo catalogue GWTC-1. The best constraints came from GW170104 and GW170823, i.e., $\Delta\gamma < 10^{-15}$.

Yu & Wang [195] and Minazzoli [196] proposed a new multimessenger test of the WEP using strongly lensed cosmic transients. By measuring the time delays between lensed images seen in different messengers, one can ob-

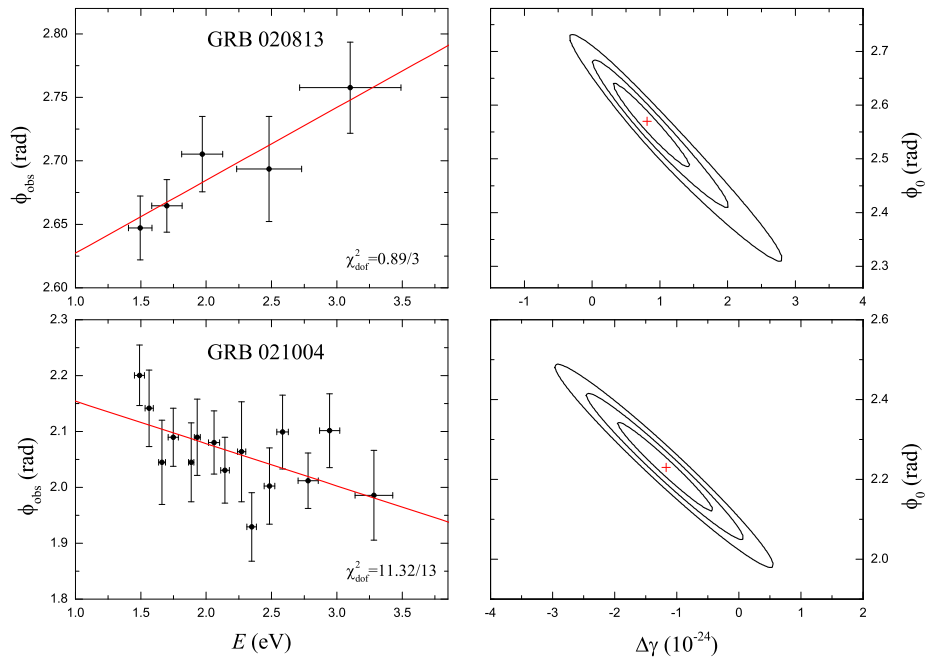


Fig. 9 Fit to the afterglow polarimetry data of GRB 020813 and GRB 021004. Left panels: linear fits of the spectropolarimetric data. Right panels: 1-3 σ confidence levels in the ϕ_0 - $\Delta\gamma$ plane. Reproduced from Ref. [198].

tain robust constraints on the differences of the γ values.

4.2 Polarization tests of the WEP

The fact that the trajectory of any freely falling test body does not depend on its internal structure is one of the consequences of the WEP. Since the polarization is viewed as a basic component of the internal structure of photons, Wu et al. [197] proposed that multiband electromagnetic emissions exploiting different polarizations are an essential tool for testing the accuracy of the WEP.

For a linearly polarized light, it is the combination of two monochromatic waves with opposite circular polarizations (labeled with ‘ l ’ and ‘ r ’). If the WEP fails, then the two circularly polarized beams travel through the same gravitational field with different Shapiro delays. The relative Shapiro delay Δt_{gra} of these two beams is the same as Eq. (30), except now $\Delta\gamma = |\gamma_l - \gamma_r|$ corresponds to the difference of the γ values for the left- and right-handed circular polarization states. Because of the arrival-time difference between the two circular components, the polarization plane of a linearly polarized light would be subject to a rotation along the photons’ propagation path. The rotation angle due to the WEP violation is given by [101, 102]

$$\Delta\phi_{\text{WEP}}(E) = \Delta t_{\text{gra}} \frac{2\pi c}{\lambda} = \Delta t_{\text{gra}} \frac{E}{\hbar}, \quad (34)$$

where E is the observed energy.

Since the initial angle of the linearly polarized light is not available, the exact value of $\Delta\phi_{\text{WEP}}$ is unknown. Yet, we can set an upper limit for the differential rotation angle $|\Delta\phi(E_2) - \Delta\phi(E_1)|$, because the polarization signal would be erased as the path difference goes beyond the coherence length. Therefore, the detection of linear polarization indicates that $|\Delta\phi(E_2) - \Delta\phi(E_1)|$ should not be too large. By considering the Shapiro delay of the Milky Way’s gravitational potential, and setting the upper limit of $|\Delta\phi(E_2) - \Delta\phi(E_1)|$ to be 2π , Yang et al. [101] obtained an upper limit on the γ discrepancy of $\Delta\gamma < 1.6 \times 10^{-27}$ from the polarization measurement of GRB 110721A.³ Through a detailed calculation on the evolution of GRB polarization arising from the WEP violation, Wei & Wu [102] proved that the initial polarization signal is not significantly suppressed even if $|\Delta\phi(E_2) - \Delta\phi(E_1)|$ is larger than $\pi/2$. Applying their formulae to the GRB polarimetric data, Wei & Wu [102] placed the most stringent limits so far on a deviation from the WEP for two cases: $\Delta\gamma < 0.8 \times 10^{-33}$ for GRB 061122 and $\Delta\gamma < 1.3 \times 10^{-33}$ for GRB 110721A.

If the rotation angle induced by the WEP violation is considered here, the observed linear polarization an-

³Similar LIV constraints have been obtained by astrophysical polarization measurements [45, 49]. Here, the LIV effect was supposed not to work simultaneously to accidentally enhance or cancel the effect from the WEP violation.

gle for photons emitted at a certain energy E with an intrinsic polarization angle ϕ_0 should be

$$\phi_{\text{obs}} = \phi_0 + \Delta\phi_{\text{WEP}}(E). \quad (35)$$

Instead of requiring the argument that the rotation of the polarization plane would severely reduce polarization over a broad bandwidth, Wei & Wu [198] simply assumed that ϕ_0 is an unknown constant. One can then constrain the WEP violation by measuring the energy-dependent change of the polarization angle. Wei & Wu [198] showed that it is possible to give constraints on both $\Delta\gamma$ and ϕ_0 through direct fitting of the multiwavelength polarimetric data of the optical afterglows of GRB 020813 and GRB 021004 (see Figure 9). At the 3σ confidence level, the joint constraint on $\Delta\gamma$ from two GRBs is $-2.7 \times 10^{-24} < \Delta\gamma < 3.1 \times 10^{-25}$. Yi et al. [199, 200] applied the same method to radio polarimetry data of the blazar 3C 279 and extragalactic radio sources, and obtained less stringent constraints on $\Delta\gamma$.

Shapiro delay-based tests of the WEP are summarized in Table 4 for comparison. When the test particles are different messengers, the best multimessenger constraint is $\Delta\gamma < 1.3 \times 10^{-13}$ for keV photons and the TeV neutrino from GRB 110521B [172]. When the test particles are the same messengers but with different energies, the best constraints are $\Delta\gamma < 2.5 \times 10^{-16}$ for 1.344–1.374 GHz photons from FRB 121102 subbursts [71] and $\Delta\gamma < 6.2 \times 10^{-16}$ for ~ 100 Hz GW signals from GW170104 [194]. When the test particles are the same messengers but with different polarization states, the best constraint is $\Delta\gamma < 0.8 \times 10^{-33}$ for polarized gamma-ray photons from GRB 061122 [102].

5 Summary and future prospect

In this paper, we have reviewed the status of the high-precision tests of fundamental physics with astrophysical transients. A few solid conclusions and future prospect can be summarized:

(i) Violations of Lorentz invariance can be tested by seeking a frequency-dependent velocity resulting from vacuum dispersion and by searching for a change in polarization arising from vacuum birefringence.

For vacuum dispersion studies, in order to obtain tighter limits on the LIV effects one should choose the waves of higher frequencies that propagate over longer distances. GRBs, with their short spectral lags, cosmological distances, and gamma-ray emissions, are the most powerful probes so far for LIV constraints in the dispersive photon sector. In the past, emission from GRBs has been observed only at energies below 100 GeV. Recently, VHE photons above 100 GeV have been detected from GRB 190114C [118] and GRB 180720B [201], opening

a new window to study GRBs in sub-TeV gamma-rays. Such detections are expected to become routine in the future [202], especially with the operations of facilities such as the international Cherenkov Telescope Array (CTA) and the Large High Altitude Air Shower Observatory (LHAASO) in China. Observations of extremely high-energy emission from more GRBs will further improve constraints on LIV. For vacuum birefringence studies, in order to tightly constrain the LIV effects one should choose those astrophysical sources with larger distances and polarization observations in a higher energy band. Thanks to their polarized gamma-ray emissions and large cosmological distances, GRBs are promising sources for seeking LIV-induced vacuum birefringence. As more and more GRB polarimeters (such as POLAR-II, TSUB-AME, NCT/COSI, GRAPE; see McConnell [203] for a review) enter service, it is reasonable to expect that the GRB polarimetric data will be significantly enlarged. Limits on the vacuum birefringent effect can be further improved with larger number of GRBs with higher energy polarimetry and higher redshifts.

(ii) The most direct and robust method for constraining the photon rest mass is to measure the frequency-dependent dispersion of light.

Theoretically speaking, to obtain more stringent bounds on the photon mass one should choose the waves of lower frequencies that propagate over longer distances. Cosmological FRBs, with their short time durations, low frequency emissions, and long propagation distances, are the most excellent astrophysical probes so far for constraining the photon mass. However, the derivation of a photon mass limit through the dispersion method is complicated by the similar frequency dependences of the dispersions due to the plasma and nonzero photon mass effects. If in the future more FRB redshifts are measured, the different redshift dependences of the plasma and photon mass contributions to the DM can be used to break dispersion degeneracy and to improve the sensitivity to the photon mass [67–69, 72, 150]. It is encouraging that radio telescopes, such as the Canadian Hydrogen Intensity Mapping Experiment (CHIME) [154], the Australia Square Kilometer Array Pathfinder (ASKAP) [155], and the Deep Synoptic Array 10-dish prototype (DSA-10) [157], have led to direct localizations of FRBs. The field will also greatly benefit from the operations of facilities, such as the Five Hundred Meter Aperture Spherical radio Telescope (FAST), the DSA-2000, and the Square Kilometer Array (SKA). The rapid progress in localizing FRBs will further improve the constraints on the photon mass. In the future, a swarm of nano-satellites orbiting the Moon will open a new window at very low frequencies in the KHz–MHz range [150]. These satellites are expected to function as a distributed low frequency array far away from the blocking ionosphere and terrestrial

radio frequency interference, which will have stable conditions for observing the cosmic signals. Such low frequency observations would offer a more sensitive probe of any delays expected from a nonzero photon mass.

(iii) Shapiro delay-based tests of the WEP have reached high precision.

Pioneered by SN 1987A tests [96, 97], the Shapiro delay experienced by an astrophysical messenger traveling through a gravitational field has been intensively employed to constrain possible violations of the WEP (e.g., [98–102]). However, there are some uncertainties and caveats involved in such tests. The large uncertainty is from the estimation of the local gravitational potential $U(r)$. The exact gravitational potential function is not well known. More accurate models of the function $U(r)$ could improve the constraints on the WEP violation, but the improvement should be very limited. Most often the Shapiro delay terms caused by the host galaxy and the intergalactic gravitational potential are ignored. In principle, these terms might be much larger than that caused by the local gravitational potential. With the better understanding of the potential functions for these terms, the WEP tests might be improved by orders of magnitude. As explained in Gao & Wald [204], Eq. (29) is gauge dependent, i.e., depending on the coordinate choice one can obtain both positive and negative values of the Shapiro delay. Additionally, Eq. (29) implicitly assumes that the trajectory is short enough that one can treat the cosmological spacetime as Minkowski plus a linear perturbation. Minazzoli et al. [167] showed that this assumption is well justified for sufficiently nearby sources like GW170817, but not for sources at cosmological distances such as GRBs or FRBs with redshifts $z \geq 1$. While Nusser [186] has provided a formulation that, in principle, can be applied to more distant sources, most of the previously cited works use the standard expression for the Shapiro delay (Eq. 29). This is an additional source of uncertainty involved in such WEP tests. The standard use of Eq. (29) also suffers from an assumption that there exists a coordinate time such that the potential and its derivative vanishes at infinity. Minazzoli et al. [167] showed that such an assumption results in a spurious divergence of the Shapiro delay for increasingly remote sources. With the use of an adequate coordinate time, Minazzoli et al. [167] found that the Shapiro delay is no longer monotonic with the number of the sources of the gravitational field. Hence, without further assumptions and/or observational input, one can not obtain a conservative lower limit on the Shapiro delay from a subset of the gravitational sources based on Eq. (29). It might be possible to constrain the gravitational potential along the line of sight using cosmological observations (e.g., of galaxy peculiar velocities, as in Ref. [205]), and thus avoid the need to use Eq. (29). Minazzoli et al. [167] suggested that any further developments of this Shapiro delay-based test should be inspired by a fundamental theory to avoid the gauge dependence of the current expression of the test.

zoli et al. [167] suggested that any further developments of this Shapiro delay-based test should be inspired by a fundamental theory to avoid the gauge dependence of the current expression of the test.

Acknowledgements We are grateful to the anonymous referees for insightful comments. This work is partially supported by the National Natural Science Foundation of China (grant Nos. 11673068, 11725314, U1831122, and 12041306), the Youth Innovation Promotion Association (2017366), the Key Research Program of Frontier Sciences (grant Nos. QYZDB-SSW-SYS005 and ZDBS-LY-7014), and the Strategic Priority Research Program “Multi-waveband gravitational wave universe” (grant No. XDB23000000) of Chinese Academy of Sciences.

References

1. R. Gambini, J. Pullin, Phys. Rev. D **59**(12), 124021 (1999). DOI 10.1103/PhysRevD.59.124021
2. J. Alfaro, H.A. Morales-Técotl, L.F. Urrutia, Phys. Rev. D **65**(10), 103509 (2002). DOI 10.1103/PhysRevD.65.103509
3. G. Amelino-Camelia, D.V. Ahluwalia, International Journal of Modern Physics D **11**(1), 35 (2002). DOI 10.1142/S0218271802001330
4. G. Amelino-Camelia, Nature **418**(6893), 34 (2002). DOI 10.1038/418034a
5. J. Kowalski-Glikman, S. Nowak, Physics Letters B **539**(1), 126 (2002). DOI 10.1016/S0370-2693(02)02063-4
6. J. Magueijo, L. Smolin, Phys. Rev. D **67**(4), 044017 (2003). DOI 10.1103/PhysRevD.67.044017
7. V.A. Kostelecký, S. Samuel, Phys. Rev. D **39**, 683 (1989). DOI 10.1103/PhysRevD.39.683
8. V.A. Kostelecký, R. Potting, Nuclear Physics B **359**, 545 (1991)
9. V.A. Kostelecký, R. Potting, Phys. Rev. D **51**, 3923 (1995). DOI 10.1103/PhysRevD.51.3923
10. D. Mattingly, Living Reviews in Relativity **8**, 5 (2005). DOI 10.12942/lrr-2005-5
11. R. Bluhm, Lecture Notes in Physics **702**, 191 (2006). DOI 10.1007/3-540-34523-X_8
12. G. Amelino-Camelia, Living Reviews in Relativity **16**, 5 (2013). DOI 10.12942/lrr-2013-5
13. J.D. Tasson, Reports on Progress in Physics **77**(6), 062901 (2014). DOI 10.1088/0034-4885/77/6/062901
14. V.A. Kostelecký, N. Russell, Reviews of Modern Physics **83**, 11 (2011). DOI 10.1103/RevModPhys.83.11

15. V.A. Kostelecký, M. Mewes, *Astrophys. J. Lett.***689**, L1 (2008). DOI 10.1086/595815
16. G. Amelino-Camelia, J. Ellis, N.E. Mavromatos, D.V. Nanopoulos, S. Sarkar, *Nature***393**, 763 (1998). DOI 10.1038/31647
17. T.G. Pavlopoulos, *Physics Letters B* **625**, 13 (2005). DOI 10.1016/j.physletb.2005.08.064
18. J. Ellis, N.E. Mavromatos, D.V. Nanopoulos, A.S. Sakharov, E.K.G. Sarkisyan, *Astroparticle Physics* **25**, 402 (2006). DOI 10.1016/j.astropartphys.2006.04.001
19. U. Jacob, T. Piran, *JCAP***1**, 031 (2008). DOI 10.1088/1475-7516/2008/01/031
20. V.A. Kostelecký, M. Mewes, *Phys. Rev. D***80**(1), 015020 (2009). DOI 10.1103/PhysRevD.80.015020
21. A.A. Abdo, M. Ackermann, M. Arimoto, et al., *Science* **323**(5922), 1688 (2009). DOI 10.1126/science.1169101
22. A.A. Abdo, M. Ackermann, M. Ajello, et al., *Nature***462**(7271), 331 (2009). DOI 10.1038/nature08574
23. Z. Chang, Y. Jiang, H.N. Lin, *Astroparticle Physics* **36**(1), 47 (2012). DOI 10.1016/j.astropartphys.2012.04.006
24. R.J. Nemiroff, R. Connolly, J. Holmes, A.B. Kostinski, *Phys. Rev. Lett.***108**(23), 231103 (2012). DOI 10.1103/PhysRevLett.108.231103
25. V. Vasileiou, A. Jacholkowska, F. Piron, J. Bolmont, C. Couturier, J. Granot, F.W. Stecker, J. Cohen-Tanugi, F. Longo, *Phys. Rev. D***87**(12), 122001 (2013). DOI 10.1103/PhysRevD.87.122001
26. J. Ellis, N.E. Mavromatos, *Astroparticle Physics* **43**, 50 (2013). DOI 10.1016/j.astropartphys.2012.05.004
27. F. Kislát, H. Krawczynski, *Phys. Rev. D***92**(4), 045016 (2015). DOI 10.1103/PhysRevD.92.045016
28. S. Zhang, B.Q. Ma, *Astroparticle Physics* **61**, 108 (2015). DOI 10.1016/j.astropartphys.2014.04.008
29. J.J. Wei, B.B. Zhang, L. Shao, X.F. Wu, P. Mészáros, *Astrophys. J. Lett.***834**(2), L13 (2017). DOI 10.3847/2041-8213/834/2/L13
30. J.J. Wei, X.F. Wu, B.B. Zhang, L. Shao, P. Mészáros, V.A. Kostelecký, *Astrophys. J.***842**(2), 115 (2017). DOI 10.3847/1538-4357/aa7630
31. J.J. Wei, X.F. Wu, *Astrophys. J.***851**(2), 127 (2017). DOI 10.3847/1538-4357/aa9d8d
32. J. Ellis, R. Konoplich, N.E. Mavromatos, L. Nguyen, A.S. Sakharov, E.K. Sarkisyan-Grinbaum, *Phys. Rev. D***99**(8), 083009 (2019). DOI 10.1103/PhysRevD.99.083009
33. V.A. Acciari, S. Ansoldi, L.A. Antonelli, et al., *Phys. Rev. Lett.* **125**, 021301 (2020). DOI 10.1103/PhysRevLett.125.021301.
34. S.D. Biller, A.C. Breslin, J. Buckley, et al., *Phys. Rev. Lett.***83**(11), 2108 (1999). DOI 10.1103/PhysRevLett.83.2108
35. P. Kaaret, *Astron. Astroph.***345**, L32 (1999)
36. S.M. Carroll, G.B. Field, R. Jackiw, *Phys. Rev. D***41**(4), 1231 (1990). DOI 10.1103/PhysRevD.41.1231
37. D. Colladay, V.A. Kostelecký, *Phys. Rev. D***58**(11), 116002 (1998). DOI 10.1103/PhysRevD.58.116002
38. R.J. Gleiser, C.N. Kozameh, *Phys. Rev. D***64**(8), 083007 (2001). DOI 10.1103/PhysRevD.64.083007
39. V.A. Kostelecký, M. Mewes, *Physical Review Letters* **87**(25), 251304 (2001). DOI 10.1103/PhysRevLett.87.251304
40. V.A. Kostelecký, M. Mewes, *Physical Review Letters* **97**(14), 140401 (2006). DOI 10.1103/PhysRevLett.97.140401
41. V.A. Kostelecký, M. Mewes, *Physical Review Letters* **99**(1), 011601 (2007). DOI 10.1103/PhysRevLett.99.011601
42. V.A. Kostelecký, M. Mewes, *Physical Review Letters* **110**(20), 201601 (2013). DOI 10.1103/PhysRevLett.110.201601
43. I.G. Mitrofanov, *Nature***426**, 139 (2003). DOI 10.1038/426139a
44. T. Jacobson, S. Liberati, D. Mattingly, F.W. Stecker, *Physical Review Letters* **93**(2), 021101 (2004). DOI 10.1103/PhysRevLett.93.021101
45. Y.Z. Fan, D.M. Wei, D. Xu, *Mon. Not. R. Astron. Soc.***376**, 1857 (2007). DOI 10.1111/j.1365-2966.2007.11576.x
46. G. Gubitosi, L. Pagano, G. Amelino-Camelia, A. Melchiorri, A. Cooray, *JCAP***8**, 021 (2009). DOI 10.1088/1475-7516/2009/08/021
47. P. Laurent, D. Götz, P. Binétruy, S. Covino, A. Fernandez-Soto, *Phys. Rev. D***83**(12), 121301 (2011). DOI 10.1103/PhysRevD.83.121301
48. F.W. Stecker, *Astroparticle Physics* **35**, 95 (2011). DOI 10.1016/j.astropartphys.2011.06.007
49. K. Toma, S. Mukohyama, D. Yonetoku, T. Murakami, S. Gunji, T. Mihara, Y. Morihara, T. Sakashita, T. Takahashi, Y. Wakashima, H. Yonemochi, N. Toukairin, *Physical Review Letters* **109**(24), 241104 (2012). DOI 10.1103/PhysRevLett.109.241104

50. D. Götz, S. Covino, A. Fernández-Soto, P. Laurent, Ž. Bošnjak, *Mon. Not. R. Astron. Soc.***431**, 3550 (2013). DOI 10.1093/mnras/stt439
51. D. Götz, P. Laurent, S. Antier, S. Covino, P. D'Avanzo, V. D'Elia, A. Melandri, *Mon. Not. R. Astron. Soc.***444**, 2776 (2014). DOI 10.1093/mnras/stu1634
52. H.N. Lin, X. Li, Z. Chang, *Mon. Not. R. Astron. Soc.***463**, 375 (2016). DOI 10.1093/mnras/stw2007
53. F. Kislat, H. Krawczynski, *Phys. Rev. D***95**(8), 083013 (2017). DOI 10.1103/PhysRevD.95.083013
54. A.S. Friedman, D. Leon, K.D. Crowley, D. Johnson, G. Teply, D. Tytler, B.G. Keating, G.M. Cole, *Phys. Rev. D***99**(3), 035045 (2019). DOI 10.1103/PhysRevD.99.035045
55. J.J. Wei, *Mon. Not. R. Astron. Soc.***485**(2), 2401 (2019). DOI 10.1093/mnras/stz594
56. A.S. Goldhaber, M.M. Nieto, *Reviews of Modern Physics* **43**(3), 277 (1971). DOI 10.1103/RevModPhys.43.277
57. L.C. Tu, J. Luo, G.T. Gillies, *Reports on Progress in Physics* **68**(1), 77 (2005). DOI 10.1088/0034-4885/68/1/R02
58. L.B. Okun, *Acta Physica Polonica B* **37**(3), 565 (2006)
59. A.S. Goldhaber, M.M. Nieto, *Reviews of Modern Physics* **82**(1), 939 (2010). DOI 10.1103/RevModPhys.82.939
60. G. Spavieri, J. Quintero, G.T. Gillies, M. Rodríguez, *European Physical Journal D* **61**(3), 531 (2011). DOI 10.1140/epjd/e2011-10508-7
61. B. Lovell, F.L. Whipple, L.H. Solomon, *Nature***202**(4930), 377 (1964). DOI 10.1038/202377a0
62. B. Warner, R.E. Nather, *Nature***222**(5189), 157 (1969). DOI 10.1038/222157b0
63. B.E. Schaefer, *Phys. Rev. Lett.***82**(25), 4964 (1999). DOI 10.1103/PhysRevLett.82.4964
64. B. Zhang, Y.T. Chai, Y.C. Zou, X.F. Wu, *Journal of High Energy Astrophysics* **11**, 20 (2016). DOI 10.1016/j.jheap.2016.07.001
65. J.J. Wei, E.K. Zhang, S.B. Zhang, X.F. Wu, *Research in Astronomy and Astrophysics* **17**(2), 13 (2017). DOI 10.1088/1674-4527/17/2/13
66. X.F. Wu, S.B. Zhang, H. Gao, J.J. Wei, Y.C. Zou, W.H. Lei, B. Zhang, Z.G. Dai, P. Mészáros, *Astrophys. J. Lett.***822**(1), L15 (2016). DOI 10.3847/2041-8205/822/1/L15
67. L. Bonetti, J. Ellis, N.E. Mavromatos, A.S. Sakharov, E.K. Sarkisyan-Grinbaum, A.D.A.M. Spallicci, *Physics Letters B* **757**, 548 (2016). DOI 10.1016/j.physletb.2016.04.035
68. L. Bonetti, J. Ellis, N.E. Mavromatos, A.S. Sakharov, E.K. Sarkisyan-Grinbaum, A.D.A.M. Spallicci, *Physics Letters B* **768**, 326 (2017). DOI 10.1016/j.physletb.2017.03.014
69. L. Shao, B. Zhang, *Phys. Rev. D***95**(12), 123010 (2017). DOI 10.1103/PhysRevD.95.123010
70. J.J. Wei, X.F. Wu, *JCAP***2018**(7), 045 (2018). DOI 10.1088/1475-7516/2018/07/045
71. N. Xing, H. Gao, J.J. Wei, Z. Li, W. Wang, B. Zhang, X.F. Wu, P. Mészáros, *Astrophys. J. Lett.***882**(1), L13 (2019). DOI 10.3847/2041-8213/ab3c5f
72. J.J. Wei, X.F. Wu, *Research in Astronomy and Astrophysics* **20**(12), 206 (2020). DOI 10.1088/1674-4527/20/12/206
73. E.R. Williams, J.E. Faller, H.A. Hill, *Phys. Rev. Lett.***26**(12), 721 (1971). DOI 10.1103/PhysRevLett.26.721
74. M.A. Chernikov, C.J. Gerber, H.R. Ott, H.J. Gerber, *Phys. Rev. Lett.***68**(23), 3383 (1992). DOI 10.1103/PhysRevLett.68.3383
75. R. Lakes, *Phys. Rev. Lett.***80**(9), 1826 (1998). DOI 10.1103/PhysRevLett.80.1826
76. A.S. Goldhaber, M.M. Nieto, *Phys. Rev. Lett.***91**(14), 149101 (2003). DOI 10.1103/PhysRevLett.91.149101
77. J. Luo, L.C. Tu, Z.K. Hu, E.J. Luan, *Phys. Rev. Lett.***90**(8), 081801 (2003). DOI 10.1103/PhysRevLett.90.081801
78. J. Luo, L.C. Tu, Z.K. Hu, E.J. Luan, *Phys. Rev. Lett.***91**(14), 149102 (2003). DOI 10.1103/PhysRevLett.91.149102
79. D.D. Lowenthal, *Phys. Rev. D***8**(8), 2349 (1973). DOI 10.1103/PhysRevD.8.2349
80. A. Accioly, R. Paszko, *Phys. Rev. D***69**(10), 107501 (2004). DOI 10.1103/PhysRevD.69.107501
81. J. Davis, L., A.S. Goldhaber, M.M. Nieto, *Phys. Rev. Lett.***35**(21), 1402 (1975). DOI 10.1103/PhysRevLett.35.1402
82. D.D. Ryutov, *Plasma Physics and Controlled Fusion* **39**, A73 (1997). DOI 10.1088/0741-3335/39/5A/008
83. D.D. Ryutov, *Plasma Physics and Controlled Fusion* **49**(12B), B429 (2007). DOI 10.1088/0741-3335/49/12B/S40

84. A. Retinò, A.D.A.M. Spallicci, A. Vaivads, *Astroparticle Physics* **82**, 49 (2016). DOI 10.1016/j.astropartphys.2016.05.006
85. Y. Yamaguchi, *Progress of Theoretical Physics Supplement* **11**, 1 (1959). DOI 10.1143/PTPS.11.1
86. G.V. Chibisov, *Uspekhi Fizicheskikh Nauk* **119**, 551 (1976)
87. E. Adelberger, G. Dvali, A. Gruzinov, *Phys. Rev. Lett.* **98**, 010402 (2007). DOI 10.1103/PhysRevLett.98.010402.
88. P. Pani, V. Cardoso, L. Gualtieri, E. Berti, A. Ishibashi, *Phys. Rev. Lett.* **109**(13), 131102 (2012). DOI 10.1103/PhysRevLett.109.131102
89. Y.P. Yang, B. Zhang, *Astrophys. J.* **842**(1), 23 (2017). DOI 10.3847/1538-4357/aa74de
90. C.M. Will, *Living Rev. Rel.* **9**, 3 (2006). DOI 10.12942/lrr-2006-3
91. C.M. Will, *Living Rev. Rel.* **17**, 4 (2014). DOI 10.12942/lrr-2014-4
92. S.B. Lambert, C. Le Poncin-Lafitte, *Astron. Astroph.* **499**(1), 331 (2009). DOI 10.1051/0004-6361/200911714
93. S.B. Lambert, C. Le Poncin-Lafitte, *Astron. Astroph.* **529**, A70 (2011). DOI 10.1051/0004-6361/201016370
94. B. Bertotti, L. Iess, P. Tortora, *Nature* **425**(6956), 374 (2003). DOI 10.1038/nature01997
95. I.I. Shapiro, *Phys. Rev. Lett.* **13**, 789 (1964). DOI 10.1103/PhysRevLett.13.789
96. M.J. Longo, *Phys. Rev. Lett.* **60**, 173 (1988). DOI 10.1103/PhysRevLett.60.173
97. L.M. Krauss, S. Tremaine, *Phys. Rev. Lett.* **60**, 176 (1988). DOI 10.1103/PhysRevLett.60.176
98. H. Gao, X.F. Wu, P. Mészáros, *Astrophys. J.* **810**, 121 (2015). DOI 10.1088/0004-637X/810/2/121
99. J.J. Wei, H. Gao, X.F. Wu, P. Mészáros, *Phys. Rev. Lett.* **115**(26), 261101 (2015). DOI 10.1103/PhysRevLett.115.261101
100. X.F. Wu, H. Gao, J.J. Wei, P. Mészáros, B. Zhang, Z.G. Dai, S.N. Zhang, Z.H. Zhu, *Phys. Rev. D* **94**(2), 024061 (2016). DOI 10.1103/PhysRevD.94.024061
101. C. Yang, Y.C. Zou, Y.Y. Zhang, B. Liao, W.H. Lei, *Mon. Not. R. Astron. Soc.* **469**, L36 (2017). DOI 10.1093/mnrasl/slx045
102. J.J. Wei, X.F. Wu, *Phys. Rev. D* **99**(10), 103012 (2019). DOI 10.1103/PhysRevD.99.103012
103. L. Smolin, arXiv e-prints hep-th/0303185 (2003)
104. C. Rovelli, *Living Reviews in Relativity* **1**(1), 1 (1998). DOI 10.12942/lrr-1998-1
105. L. Burderi, A. Sanna, T. Di Salvo, L. Amati, G. Amelino-Camelia, M. Branchesi, S. Capozziello, E. Coccia, M. Colpi, E. Costa, N. D'Amico, P. De Bernardis, M. De Laurentis, M. Della Valle, H. Falcke, M. Feroci, F. Fiore, F. Frontera, A.F. Gambino, G. Ghisellini, K. Hurley, R. Iaria, D. Kataria, C. Labanti, G. Lodato, B. Negri, A. Papitto, T. Piran, A. Riggio, C. Rovelli, A. Santangelo, F. Vidotto, S. Zane, arXiv e-prints arXiv:1911.02154 (2019)
106. J. Ellis, N.E. Mavromatos, D.V. Nanopoulos, A.S. Sakharov, E.K.G. Sarkisyan, *Astroparticle Physics* **29**(2), 158 (2008). DOI 10.1016/j.astropartphys.2007.12.003
107. J. Ellis, N.E. Mavromatos, D.V. Nanopoulos, A.S. Sakharov, *Astron. Astroph.* **402**, 409 (2003). DOI 10.1051/0004-6361:20030263
108. S.E. Boggs, C.B. Wunderer, K. Hurley, W. Coburn, *Astrophys. J. Lett.* **611**(2), L77 (2004). DOI 10.1086/423933
109. M. Rodríguez Martínez, T. Piran, Y. Oren, *JCAP* **2006**(5), 017 (2006). DOI 10.1088/1475-7516/2006/05/017
110. J. Bolmont, A. Jacholkowska, J.L. Atteia, F. Piron, G. Pizzichini, *Astrophys. J.* **676**(1), 532 (2008). DOI 10.1086/527524
111. R. Lamon, N. Produit, F. Steiner, *General Relativity and Gravitation* **40**(8), 1731 (2008). DOI 10.1007/s10714-007-0580-6
112. Z. Xiao, B.Q. Ma, *Phys. Rev. D* **80**(11), 116005 (2009). DOI 10.1103/PhysRevD.80.116005
113. L. Shao, Z. Xiao, B.Q. Ma, *Astroparticle Physics* **33**(5-6), 312 (2010). DOI 10.1016/j.astropartphys.2010.03.003
114. H. Xu, B.Q. Ma, *Astroparticle Physics* **82**, 72 (2016). DOI 10.1016/j.astropartphys.2016.05.008
115. H. Xu, B.Q. Ma, *Physics Letters B* **760**, 602 (2016). DOI 10.1016/j.physletb.2016.07.044
116. H. Xu, B.Q. Ma, *JCAP* **2018**(1), 050 (2018). DOI 10.1088/1475-7516/2018/01/050
117. Y. Liu, B.Q. Ma, *The European Physical Journal C* **78**(10), 825 (2018). DOI 10.1140/epjc/s10052-018-6294-y.
118. MAGIC Collaboration, V.A. Acciari, S. Ansoldi, et al., *Nature* **575**(7783), 455 (2019). DOI 10.1038/s41586-019-1750-x
119. M. Biesiada, A. Piórkowska, *Classical and Quantum Gravity* **26**(12), 125007 (2009). DOI 10.1088/0264-9381/26/12/125007

120. Y. Pan, Y. Gong, S. Cao, H. Gao, Z.H. Zhu, *Astrophys. J.***808**(1), 78 (2015). DOI 10.1088/0004-637X/808/1/78
121. X.B. Zou, H.K. Deng, Z.Y. Yin, H. Wei, *Physics Letters B* **776**, 284 (2018). DOI 10.1016/j.physletb.2017.11.053
122. Y. Pan, J. Qi, S. Cao, T. Liu, Y. Liu, S. Geng, Y. Lian, Z.H. Zhu, *Astrophys. J.***890**(2), 169 (2020). DOI 10.3847/1538-4357/ab6ef5
123. T.N. Ukwatta, K.S. Dhuga, M. Stamatikos, C.D. Dermer, T. Sakamoto, E. Sonbas, W.C. Parke, L.C. Maximon, J.T. Linnemann, P.N. Bhat, A. Eskandarian, N. Gehrels, A.U. Abeysekara, K. Tollefson, J.P. Norris, *Mon. Not. R. Astron. Soc.***419**(1), 614 (2012). DOI 10.1111/j.1365-2966.2011.19723.x
124. M.G. Bernardini, G. Ghirlanda, S. Campana, S. Covino, R. Salvaterra, J.L. Atteia, D. Burlon, G. Calderone, P. D'Avanzo, V. D'Elia, G. Ghisellini, V. Heussaff, D. Lazzati, A. Melandri, L. Nava, S.D. Vergani, G. Tagliaferri, *Mon. Not. R. Astron. Soc.***446**(2), 1129 (2015). DOI 10.1093/mnras/stu2153
125. Z. Chang, X. Li, H.N. Lin, Y. Sang, P. Wang, S. Wang, *Chinese Physics C* **40**(4), 045102 (2016). DOI 10.1088/1674-1137/40/4/045102
126. L. Shao, B.B. Zhang, F.R. Wang, X.F. Wu, Y.H. Cheng, X. Zhang, B.Y. Yu, B.J. Xi, X. Wang, H.X. Feng, M. Zhang, D. Xu, *Astrophys. J.***844**(2), 126 (2017). DOI 10.3847/1538-4357/aa7d01
127. R.J. Lu, Y.F. Liang, D.B. Lin, J. Lü, X.G. Wang, H.J. Lü, H.B. Liu, E.W. Liang, B. Zhang, *Astrophys. J.***865**(2), 153 (2018). DOI 10.3847/1538-4357/aada16
128. MAGIC Collaboration, J. Albert, E. Aliu, et al., *Physics Letters B* **668**, 253 (2008). DOI 10.1016/j.physletb.2008.08.053
129. M. Martínez, M. Errando, *Astroparticle Physics* **31**(3), 226 (2009). DOI 10.1016/j.astropartphys.2009.01.005
130. H. Abdalla, F. Aharonian, F. Ait Benkhali, et al., *Astrophys. J.***870**(2), 93 (2019). DOI 10.3847/1538-4357/aaf1c4
131. F. Aharonian, A.G. Akhperjanian, U. Barres de Almeida, et al., *Physical Review Letters* **101**(17), 170402 (2008). DOI 10.1103/PhysRevLett.101.170402
132. H. E. S. S. Collaboration, A. Abramowski, F. Acero, et al., *Astroparticle Physics* **34**(9), 738 (2011). DOI 10.1016/j.astropartphys.2011.01.007
133. N. OTTE, in *International Cosmic Ray Conference, International Cosmic Ray Conference*, vol. 7 (2011), *International Cosmic Ray Conference*, vol. 7, p. 256. DOI 10.7529/ICRC2011/V07/1302
134. B. Zitzer, VERITAS Collaboration, in *International Cosmic Ray Conference, International Cosmic Ray Conference*, vol. 33 (2013), *International Cosmic Ray Conference*, vol. 33, p. 2768
135. MAGIC Collaboration, M.L. Ahnen, S. Ansoldi, et al., *Astrophys. J. Suppl.***232**(1), 9 (2017). DOI 10.3847/1538-4365/aa8404
136. R.C. Myers, M. Pospelov, *Physical Review Letters* **90**(21), 211601 (2003). DOI 10.1103/PhysRevLett.90.211601
137. W. Coburn, S.E. Boggs, *Nature***423**, 415 (2003). DOI 10.1038/nature01612
138. R.E. Rutledge, D.B. Fox, *Mon. Not. R. Astron. Soc.***350**, 1288 (2004). DOI 10.1111/j.1365-2966.2004.07665.x
139. C. Wigger, W. Hajdas, K. Arzner, M. Güdel, A. Zehnder, *Astrophys. J.***613**, 1088 (2004). DOI 10.1086/423163
140. L. Maccione, S. Liberati, A. Celotti, J.G. Kirk, P. Ubertini, *Phys. Rev. D***78**(10), 103003 (2008). DOI 10.1103/PhysRevD.78.103003
141. E. Kalemci, S.E. Boggs, C. Kouveliotou, M. Finger, M.G. Baring, *Astrophys. J. Suppl.***169**, 75 (2007). DOI 10.1086/510676
142. S. McGlynn, D.J. Clark, A.J. Dean, L. Hanlon, S. McBreen, D.R. Willis, B. McBreen, A.J. Bird, S. Foley, *Astron. Astroph.***466**, 895 (2007). DOI 10.1051/0004-6361:20066179
143. D. Götz, P. Laurent, F. Lebrun, F. Daigne, Ž. Bošnjak, *Astrophys. J. Lett.***695**, L208 (2009). DOI 10.1088/0004-637X/695/2/L208
144. D. Yonetoku, T. Murakami, S. Gunji, T. Mihara, K. Toma, T. Sakashita, Y. Morihara, T. Takahashi, N. Toukairin, H. Fujimoto, Y. Kodama, S. Kubo, IKAROS Demonstration Team, *Astrophys. J. Lett.***743**, L30 (2011). DOI 10.1088/2041-8205/743/2/L30
145. D. Yonetoku, T. Murakami, S. Gunji, T. Mihara, K. Toma, Y. Morihara, T. Takahashi, Y. Wakashima, H. Yonemochi, T. Sakashita, N. Toukairin, H. Fujimoto, Y. Kodama, *Astrophys. J. Lett.***758**, L1 (2012). DOI 10.1088/2041-8205/758/1/L1
146. H.K. Vedantham, V. Ravi, K. Mooley, D. Frail, G. Hallinan, S.R. Kulkarni, *Astrophys. J. Lett.***824**(1), L9 (2016). DOI 10.3847/2041-8205/824/1/L9

147. P.K.G. Williams, E. Berger, *Astrophys. J. Lett.***821**(2), L22 (2016). DOI 10.3847/2041-8205/821/2/L22
148. S. Chatterjee, C.J. Law, R.S. Wharton, S. Burke-Spolaor, J.W.T. Hessels, G.C. Bower, J.M. Cordes, S.P. Tendulkar, C.G. Bassa, P. Demorest, B.J. Butler, A. Seymour, P. Scholz, M.W. Abruzzo, S. Bogdanov, V.M. Kaspi, A. Keimpema, T.J.W. Lazio, B. Marcote, M.A. McLaughlin, Z. Paragi, S.M. Ransom, M. Rupen, L.G. Spitler, H.J. van Langevelde, *Nature***541**(7635), 58 (2017). DOI 10.1038/nature20797
149. J.W.T. Hessels, L.G. Spitler, A.D. Seymour, J.M. Cordes, D. Michilli, R.S. Lynch, K. Gourdji, A.M. Archibald, C.G. Bassa, G.C. Bower, S. Chatterjee, L. Connor, F. Crawford, J.S. Deneva, V. Gajjar, V.M. Kaspi, A. Keimpema, C.J. Law, B. Marcote, M.A. McLaughlin, Z. Paragi, E. Petroff, S.M. Ransom, P. Scholz, B.W. Stappers, S.P. Tendulkar, *Astrophys. J. Lett.***876**(2), L23 (2019). DOI 10.3847/2041-8213/ab13ae
150. M.J. Bentum, L. Bonetti, A.R.D.A.M. Spallicci, *Advances in Space Research* **59**(2), 736 (2017). DOI 10.1016/j.asr.2016.10.018
151. W. Deng, B. Zhang, *Astrophys. J. Lett.***783**(2), L35 (2014). DOI 10.1088/2041-8205/783/2/L35
152. L.G. Spitler, P. Scholz, J.W.T. Hessels, S. Bogdanov, A. Brazier, F. Camilo, S. Chatterjee, J.M. Cordes, F. Crawford, J. Deneva, R.D. Ferdman, P.C.C. Freire, V.M. Kaspi, P. Lazarus, R. Lynch, E.C. Madsen, M.A. McLaughlin, C. Patel, S.M. Ransom, A. Seymour, I.H. Stairs, B.W. Stappers, J. van Leeuwen, W.W. Zhu, *Nature***531**(7593), 202 (2016). DOI 10.1038/nature17168
153. S.P. Tendulkar, C.G. Bassa, J.M. Cordes, G.C. Bower, C.J. Law, S. Chatterjee, E.A.K. Adams, S. Bogdanov, S. Burke-Spolaor, B.J. Butler, P. Demorest, J.W.T. Hessels, V.M. Kaspi, T.J.W. Lazio, N. Maddox, B. Marcote, M.A. McLaughlin, Z. Paragi, S.M. Ransom, P. Scholz, A. Seymour, L.G. Spitler, H.J. van Langevelde, R.S. Wharton, *Astrophys. J. Lett.***834**(2), L7 (2017). DOI 10.3847/2041-8213/834/2/L7
154. B. Marcote, K. Nimmo, J.W.T. Hessels, et al., *Nature***577**(7789), 190 (2020). DOI 10.1038/s41586-019-1866-z
155. K.W. Bannister, A.T. Deller, C. Phillips, et al., *Science* **365**(6453), 565 (2019). DOI 10.1126/science.aaw5903
156. J.X. Prochaska, J.P. Macquart, M. McQuinn, S. Simha, R.M. Shannon, C.K. Day, L. Marnoch, S. Ryder, A. Deller, K.W. Bannister, S. Bhandari, R. Bordoloi, J. Bunton, H. Cho, C. Flynn, E.K. Mahony, C. Phillips, H. Qiu, N. Tejos, *Science* **366**(6462), 231 (2019). DOI 10.1126/science.aay0073
157. V. Ravi, M. Catha, L. D'Addario, S.G. Djorgovski, G. Hallinan, R. Hobbs, J. Kocz, S.R. Kulkarni, J. Shi, H.K. Vedantham, S. Weinreb, D.P. Woody, *Nature***572**(7769), 352 (2019). DOI 10.1038/s41586-019-1389-7
158. J.P. Macquart, J.X. Prochaska, M. McQuinn, K.W. Bannister, S. Bhandari, C.K. Day, A.T. Deller, R.D. Ekers, C.W. James, L. Marnoch, S. Osłowski, C. Phillips, S.D. Ryder, D.R. Scott, R.M. Shannon, N. Tejos, *Nature***581**(7809), 391 (2020). DOI 10.1038/s41586-020-2300-2
159. J.X. Prochaska, Y. Zheng, *Mon. Not. R. Astron. Soc.***485**(1), 648 (2019). DOI 10.1093/mnras/stz261
160. J. Xu, J.L. Han, *Research in Astronomy and Astrophysics* **15**(10), 1629 (2015). DOI 10.1088/1674-4527/15/10/002
161. R. Luo, K. Lee, D.R. Lorimer, B. Zhang, *Mon. Not. R. Astron. Soc.***481**(2), 2320 (2018). DOI 10.1093/mnras/sty2364
162. A.M. Hopkins, J.F. Beacom, *Astrophys. J.***651**(1), 142 (2006). DOI 10.1086/506610
163. L.X. Li, *Mon. Not. R. Astron. Soc.***388**(4), 1487 (2008). DOI 10.1111/j.1365-2966.2008.13488.x
164. Planck Collaboration, N. Aghanim, Y. Akrami, et al., *Astron. Astroph.***641**, A6 (2020). DOI 10.1051/0004-6361/201833910
165. M. Fukugita, C.J. Hogan, P.J.E. Peebles, *Astrophys. J.***503**(2), 518 (1998). DOI 10.1086/306025
166. R.B. Tully, H. Courtois, Y. Hoffman, D. Pomarède, *Nature* **513**, 71 (2014). DOI 10.1038/nature13674
167. O. Minazzoli, N.K. Johnson-McDaniel, M. Sakellariadou, *Phys. Rev. D***100**(10), 104047 (2019). DOI 10.1103/PhysRevD.100.104047
168. Z.Y. Wang, R.Y. Liu, X.Y. Wang, *Phys. Rev. Lett.* **116**(15), 151101 (2016). DOI 10.1103/PhysRevLett.116.151101
169. S. Boran, S. Desai, E.O. Kahya, *European Physical Journal C* **79**(3), 185 (2019). DOI 10.1140/epjc/s10052-019-6695-6
170. R. Laha, *Phys. Rev. D***100**(10), 103002 (2019). DOI 10.1103/PhysRevD.100.103002
171. J.J. Wei, B.B. Zhang, L. Shao, H. Gao, Y. Li, Q.Q. Yin, X.F. Wu, X.Y. Wang, B. Zhang, Z.G. Dai, *Journal of High Energy Astrophysics* **22**, 1 (2019). DOI 10.1016/j.jheap.2019.01.002

172. J.J. Wei, X.F. Wu, H. Gao, P. Mészáros, JCAP **8**, 031 (2016). DOI 10.1088/1475-7516/2016/08/031
173. X. Li, Y.M. Hu, Y.Z. Fan, D.M. Wei, Astrophys. J. **827**, 75 (2016). DOI 10.3847/0004-637X/827/1/75
174. B.P. Abbott, R. Abbott, T.D. Abbott, F. Acernese, K. Ackley, C. Adams, T. Adams, P. Addesso, R.X. Adhikari, V.B. Adya, et al., Astrophys. J. **848**, L13 (2017). DOI 10.3847/2041-8213/aa920c
175. M. Liu, Z. Zhao, X. You, J. Lu, L. Xu, Phys. Lett. B **770**, 8 (2017). DOI 10.1016/j.physletb.2017.04.033
176. H. Wang, F.W. Zhang, Y.Z. Wang, Z.Q. Shen, Y.F. Liang, X. Li, N.H. Liao, Z.P. Jin, Q. Yuan, Y.C. Zou, Y.Z. Fan, D.M. Wei, Astrophys. J. **851**, L18 (2017). DOI 10.3847/2041-8213/aa9e08
177. J.J. Wei, B.B. Zhang, X.F. Wu, H. Gao, P. Mészáros, B. Zhang, Z.G. Dai, S.N. Zhang, Z.H. Zhu, JCAP **11**, 035 (2017). DOI 10.1088/1475-7516/2017/11/035
178. I.M. Shoemaker, K. Murase, Phys. Rev. D **97**(8), 083013 (2018). DOI 10.1103/PhysRevD.97.083013
179. S. Boran, S. Desai, E.O. Kahya, R.P. Woodard, Phys. Rev. D **97**(4), 041501 (2018). DOI 10.1103/PhysRevD.97.041501
180. L. Yao, Z. Zhao, Y. Han, J. Wang, T. Liu, M. Liu, Astrophys. J. **900**(1), 31 (2020). DOI 10.3847/1538-4357/abab02
181. C. Sivaram, Bulletin of the Astronomical Society of India **27**, 627 (1999)
182. Y. Sang, H.N. Lin, Z. Chang, Mon. Not. R. Astron. Soc. **460**, 2282 (2016). DOI 10.1093/mnras/stw1136
183. Z.X. Luo, B. Zhang, J.J. Wei, X.F. Wu, JHEAp **9**, 35 (2016). DOI 10.1016/j.jheap.2016.04.001
184. H. Yu, S.Q. Xi, F.Y. Wang, Astrophys. J. **860**, 173 (2018). DOI 10.3847/1538-4357/aac2e3
185. S.J. Tingay, D.L. Kaplan, Astrophys. J. **820**, L31 (2016). DOI 10.3847/2041-8205/820/2/L31
186. A. Nusser, Astrophys. J. **821**, L2 (2016). DOI 10.3847/2041-8205/821/1/L2
187. D. Wang, Z. Li, J. Zhang, Physics of the Dark Universe **29**, 100571 (2020). DOI 10.1016/j.dark.2020.100571
188. J.J. Wei, J.S. Wang, H. Gao, X.F. Wu, Astrophys. J. **818**, L2 (2016). DOI 10.3847/2041-8205/818/1/L2
189. Y.P. Yang, B. Zhang, Phys. Rev. D **94**(10), 101501 (2016). DOI 10.1103/PhysRevD.94.101501
190. Y. Zhang, B. Gong, Astrophys. J. **837**, 134 (2017). DOI 10.3847/1538-4357/aa61fb
191. S. Desai, E. Kahya, European Physical Journal C **78**, 86 (2018). DOI 10.1140/epjc/s10052-018-5571-0
192. C. Leung, B. Hu, S. Harris, A. Brown, J. Gallicchio, H. Nguyen, Astrophys. J. **861**, 66 (2018). DOI 10.3847/1538-4357/aac954
193. E.O. Kahya, S. Desai, Phys. Lett. B **756**, 265 (2016). DOI 10.1016/j.physletb.2016.03.033
194. S.C. Yang, W.B. Han, G. Wang, Mon. Not. R. Astron. Soc. **499**(1), L53 (2020). DOI 10.1093/mnras/slaa143
195. H. Yu, F.Y. Wang, European Physical Journal C **78**(9), 692 (2018). DOI 10.1140/epjc/s10052-018-6162-9
196. O. Minazzoli, arXiv e-prints arXiv:1912.06891 (2019)
197. X.F. Wu, J.J. Wei, M.X. Lan, H. Gao, Z.G. Dai, P. Mészáros, Phys. Rev. D **95**(10), 103004 (2017). DOI 10.1103/PhysRevD.95.103004
198. J.J. Wei, X.F. Wu, European Physical Journal Plus **135**(6), 527 (2020). DOI 10.1140/epjp/s13360-020-00554-x
199. S.X. Yi, Y.C. Zou, X. Yang, B. Liao, S.W. Wei, Mon. Not. R. Astron. Soc. **493**(2), 1782 (2020). DOI 10.1093/mnras/staa369
200. S.X. Yi, Y.C. Zou, J.J. Wei, Q.Q. Zhou, Mon. Not. R. Astron. Soc. **498**(3), 4295 (2020). DOI 10.1093/mnras/staa2686
201. H. Abdalla, R. Adam, F. Aharonian, et al., Nature **575**(7783), 464 (2019). DOI 10.1038/s41586-019-1743-9
202. B. Zhang, Nature **575**(7783), 448 (2019). DOI 10.1038/d41586-019-03503-6
203. M.L. McConnell, New Astron. Rev. **76**, 1 (2017). DOI 10.1016/j.newar.2016.11.001
204. S. Gao, R.M. Wald, Classical and Quantum Gravity **17**(24), 4999 (2000). DOI 10.1088/0264-9381/17/24/305
205. Y. Hoffman, D. Pomarède, R.B. Tully, H.M. Courtois, Nature Astronomy **1**, 0036 (2017). DOI 10.1038/s41550-016-0036

Table 4 Upper constraints on the differences of the γ values through the Shapiro (gravitational) time delay effect.

Categorization	Author (year)	Source	Messengers	Gravitational Field	$\Delta\gamma$	Refs.
Different messengers	Longo (1988)	SN 1987A	eV photons and MeV neutrinos	Milky Way	3.4×10^{-3}	[96]
	Krauss and Tremaine (1988)	SN 1987A	eV photons and MeV neutrinos	Milky Way	5.0×10^{-3}	[97]
	Wang et al. (2016)	PKS B1424-418	MeV photons and PeV neutrino	Virgo Cluster	3.4×10^{-4}	[168]
		PKS B1424-418	MeV photons and PeV neutrino	Great Attractor	7.0×10^{-6}	
	Boran et al. (2019)	TXS 0506+056	GeV photons and TeV neutrino	Milky Way	5.5×10^{-2}	[169]
	Laha (2019); Wei et al. (2019)	TXS 0506+056	GeV photons and TeV neutrino	Laniakea supercluster of galaxies	$10^{-6}-10^{-7}$	[170, 171]
	Wei et al. (2016a)	GRB 110521B	keV photons and TeV neutrino	Laniakea supercluster of galaxies	1.3×10^{-13}	
	Abbott et al. (2017)	GW170817	MeV photons and GW signals	Milky Way	$-2.6 \times 10^{-7}-1.2 \times 10^{-6}$	[174]
	Wei et al. (2017)	GW170817	MeV photons and GW signals	Virgo Cluster	9.2×10^{-11}	[177]
		GW170817	eV photons and GW signals	Virgo Cluster	2.1×10^{-6}	
	Shoemaker and Murase (2018)	GW170817	MeV photons and GW signals	Milky Way	7.4×10^{-8}	[178]
	Boran et al. (2018)	GW170817	MeV photons and GW signals	Milky Way	9.8×10^{-8}	[179]
	Yao et al. (2020)	GW170817	MeV photons and GW signals	Milky Way + host galaxy	$\sim 10^{-9}$	[180]
		GW170817	eV photons and GW signals	Milky Way + host galaxy	$\sim 10^{-4}$	
Same messengers with different energies	Longo (1988)	SN 1987A	7.5–40 MeV neutrinos	Milky Way	1.6×10^{-6}	[96]
	Wei et al. (2019)	TXS 0506+056	0.1–20 TeV neutrinos	Laniakea supercluster of galaxies	7.3×10^{-6}	[171]
	Sivaram (1999)	GRB 990123	eV–MeV photons	Milky Way	4.0×10^{-7}	[181]
		GRB 090510	MeV–GeV photons	Milky Way	2.0×10^{-8}	
	Gao et al. (2015)	GRB 080319B	eV–MeV photons	Milky Way	1.2×10^{-7}	[98]
		FRB 110220	1.2–1.5 GHz photons	Milky Way	2.5×10^{-8}	
		FRB/GRB 100704A	1.23–1.45 GHz photons	Milky Way	4.4×10^{-9}	
	Wei et al. (2015)	FRB 150418	1.2–1.5 GHz photons	Milky Way	$(1-2) \times 10^{-9}$	[185]
	Tingay and Kaplan (2016)		1.2–1.5 GHz photons	Large-scale structure	$10^{-12}-10^{-13}$	
	Nusser (2016)	FRB 150418	1.2–1.5 GHz photons	Laniakea supercluster of galaxies	2.5×10^{-16}	[186]
	Xing et al. (2019)	FRB 121102 subbursts	1.344–1.374 GHz photons	Laniakea supercluster of galaxies	2.5×10^{-16}	[71]
	Wei et al. (2016b)	Mrk 421	keV–TeV photons	Milky Way	3.9×10^{-3}	[188]
		PKS 2155-304	sub TeV–TeV photons	Milky Way	2.2×10^{-6}	
	Yang and Zhang (2016)	Crab pulsar	8.15–10.35 GHz photons	Milky Way	$(0.6-1.8) \times 10^{-15}$	[189]
	Zhang and Gong (2017)	Crab pulsar	eV–MeV photons	Milky Way	3.0×10^{-10}	[190]
	Desai and Kahya (2018)	Crab pulsar	8.15–10.35 GHz photons	Milky Way	2.4×10^{-15}	[191]
	Leung et al. (2018)	Crab pulsar	1.52–2.12 eV photons	Milky Way	1.1×10^{-10}	[192]
	Wu et al. (2016)	GW150914	35–150 Hz GW signals	Milky Way	$\sim 10^{-9}$	[100]
	Kahya and Desai (2016)	GW150914	35–250 Hz GW signals	Milky Way	2.6×10^{-9}	[193]
	Yang et al. (2020)	GW170104	~ 100 Hz GW signals	Milky Way	6.2×10^{-16}	[194]
		GW170823	~ 100 Hz GW signals	Milky Way	1.0×10^{-15}	
Same messengers with different polarization states	Wu et al. (2017)	FRB 150807	Polarized radio photons	Laniakea supercluster of galaxies	2.2×10^{-16}	[197]
		GRB 120308A	Polarized optical photons	Laniakea supercluster of galaxies	1.2×10^{-10}	
		GRB 100826A	Polarized gamma-ray photons	Laniakea supercluster of galaxies	1.2×10^{-10}	
	Yang et al. (2017)	GRB 110721A	Polarized gamma-ray photons	Milky Way	1.6×10^{-27}	[101]
	Wei and Wu (2019)	GRB 061122	Polarized gamma-ray photons	Laniakea supercluster of galaxies	0.8×10^{-33}	[102]
		GRB 110721A	Polarized gamma-ray photons	Laniakea supercluster of galaxies	1.3×10^{-33}	
	Wei and Wu (2020)	GRB 020813 and GRB 021004	Polarized optical photons	Milky Way	$-2.7 \times 10^{-24}-3.1 \times 10^{-25}$	[198]